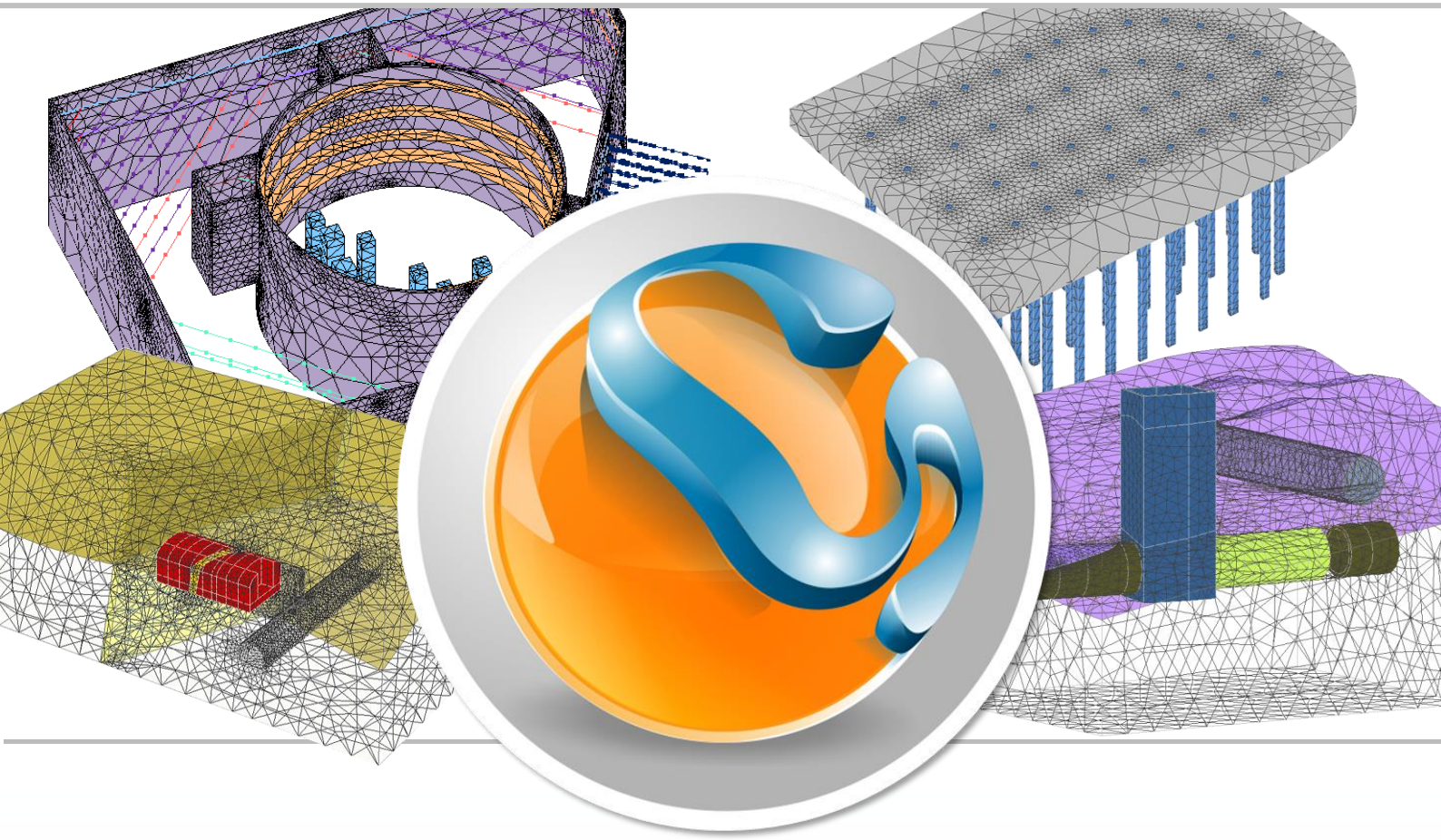

Redefining simplicity for geotechnical engineers

geofea®

VERSION 9.0

# VERIFICATION HANDBOOK

This is a verification handbook provides various test problems for GeoFEA®.

# Preface

This volume contains standard analyses used to verify that the model implementation accurately represents the developer's conceptual description and specification. Verification provides evidence that the model is solved correctly and quantify uncertainties and errors in the computational model.

**Our Goals**

- Identify and minimize uncertainties and errors in the computational model
- Increase confidence in the quantitative predictive capability of the computational model

**Our Strategy**

- Reduce computational model uncertainties and errors
- Reduce systematic errors in hardware
- Reduce incomplete physical characterization

Verification of the problem does not directly make a claim about the accuracy of a prediction as the computational models are easily misused whether intentionally or unintentionally. The user must be aware of the following:

- How closely related are the conditions of the prediction and specific cases in validation database?
- How well is the physics and characteristics of the problem understood?

Verified and validated models can be used for assessing behavior of components or complete systems, with the understanding that the environmental influences cannot all be taken into the account prior to operation but with a good model, their influence on system behavior can be assessed as need be.

# Table of Contents

**Preface** i

**Table of Contents** ii

**Problem #1: 3-D Cantilever Beam deflection** 3

1.1 Nodal loading on Euler-Bernoulli beam elements 3

1.2 Beam with 11 integration points Tetrahedral elements 4

**Problem #2: Strip load on elastic Gibson soil** 5

**Problem #3: 1-D consolidation** 9

**Problem #4: Cryer's consolidation sphere** 12

4.1 Axisymmetry modeling of Cryer's consolidation problem 14

4.2 3-D modeling of Cryer's consolidation problem 16

**Problem #5: Cylindrical Hole in an Infinite Space Using Mohr-Coulomb Material** 19

**Problem #6: Triaxial Compression Test on a Cam-Clay Sample** 26

6.1 Drained test 27

6.2 Undrained test 30

# 3-D Cantilever Beam deflection

**To verify and validate:** point load, beam element, tetrahedral element, elastic model.

| | | |
|---|---|---|
| Modulus of elasticity | : | E = 1000000 kPa |
| Height of cross section area | : | h = 1 m |
| Poisson's ratio | : | $\nu$ = 0.3 |
| Cross sectional area | : | A = h × b = 1 $m^2$ |
| Second moment of area | : | I = b × $h^3$/12 = 0.0833333 $m^4$ |
| Length of beam | : | L = 10 m |
| Applied nodal load | : | P=10 kN |

## 1.1 Nodal loading on Euler-Bernoulli beam elements

Theoretical solution for beam bending due to effect of normal stresses (Beer and Johnston, 1992):

$$\delta_{tip} = \frac{PL^3}{3EI} = 0.04\,\text{m}$$

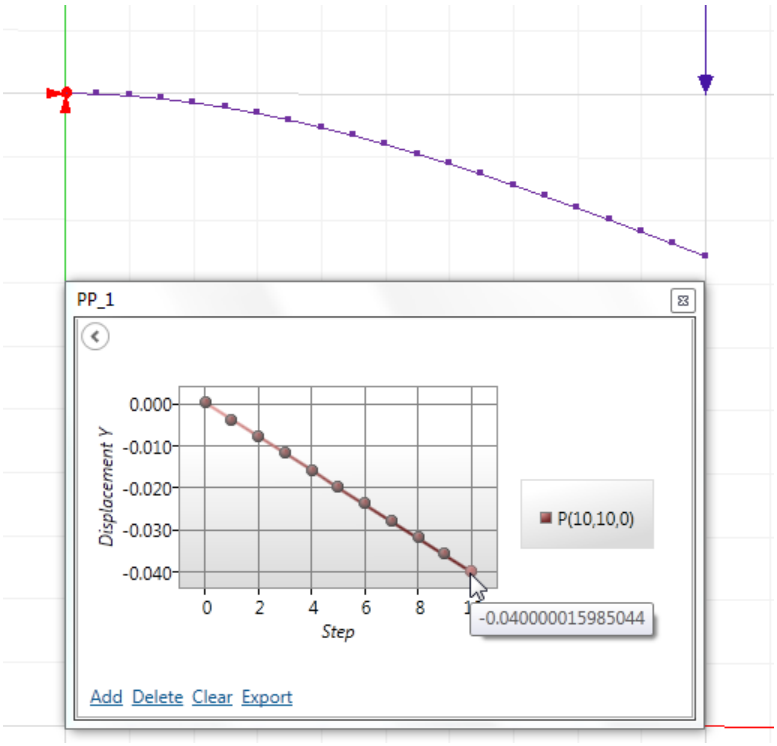


Figure 1-1 Deflection of an Euler-Bernoulli beam under a point load

## 1.2 Beam with 11 integration points Tetrahedral elements

Given the aspect ratio of the beam is 1:10, the cantilever beam is remodelled with tetrahedral elements to account for the extra rotation due to the transverse shear effects. Theoretical solution for beam bending due to effect of normal and shearing stresses (Beer and Johnston, 1992):

$$\delta_{tip} = \frac{PL^3}{3EI}\left[1 + \frac{3h^2(1+\nu)}{5L^2}\right] = 0.040312\,\text{m}$$

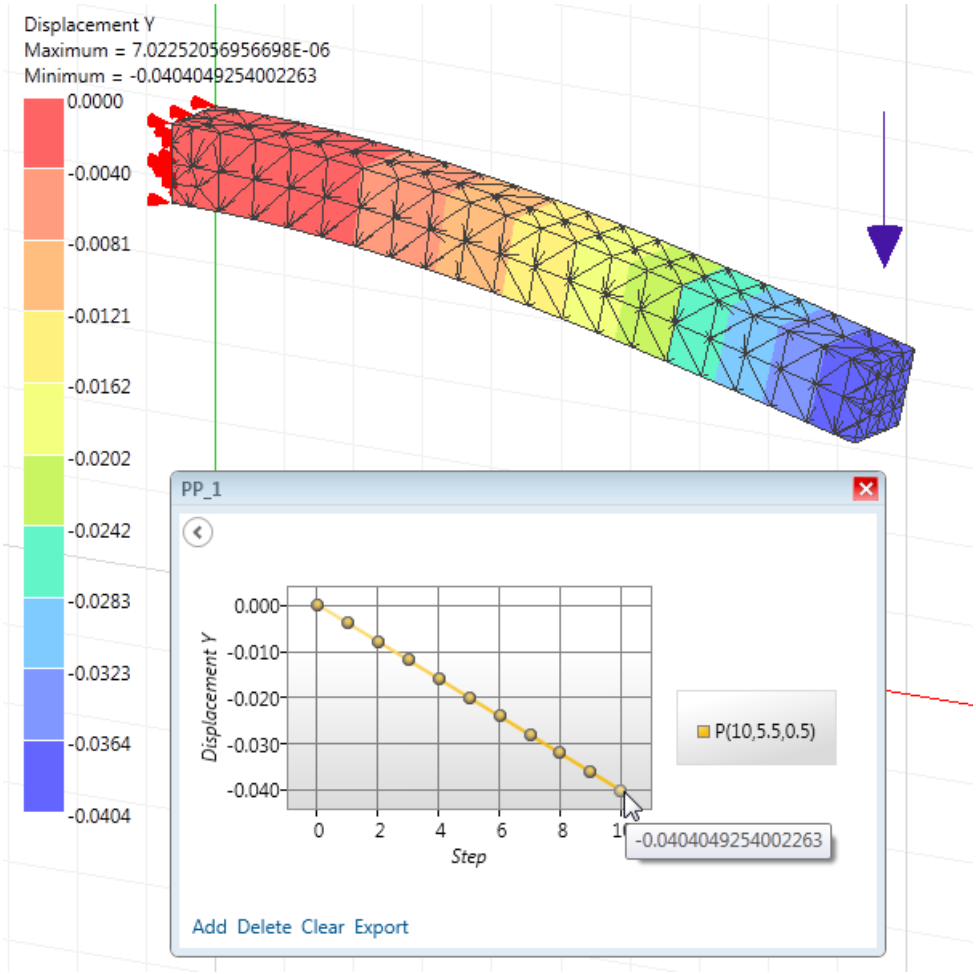


Figure 1-2 Deflection of a Timoshenko beam under a point load

***Reference:***

Beer, F. P. and Johnston, E.R. Jr., Mechanics of Material (2nd Edn), McGraw Hill International (UK) Limited, Berkshire, 1992.

# Strip load on elastic Gibson soil

**To verify and validate:** plane strain, elastic model, boundary fixities

The analytical solution is exact only for an infinite half-space whereas GeoFEA solution is obtained for soil domain with finite depth. In this current problem, the shear modulus of the soil increases linearly with depth, thus the effect of finite thickness is expected to diminish rapidly if the mesh boundary is sufficiently far.

Four meshes of different sizes is used to verify the convergence of the results towards analytical solution. The exact solution gives a settlement of 0.05m (Gibson, 1967) at the surface below the centre of the distributed load.

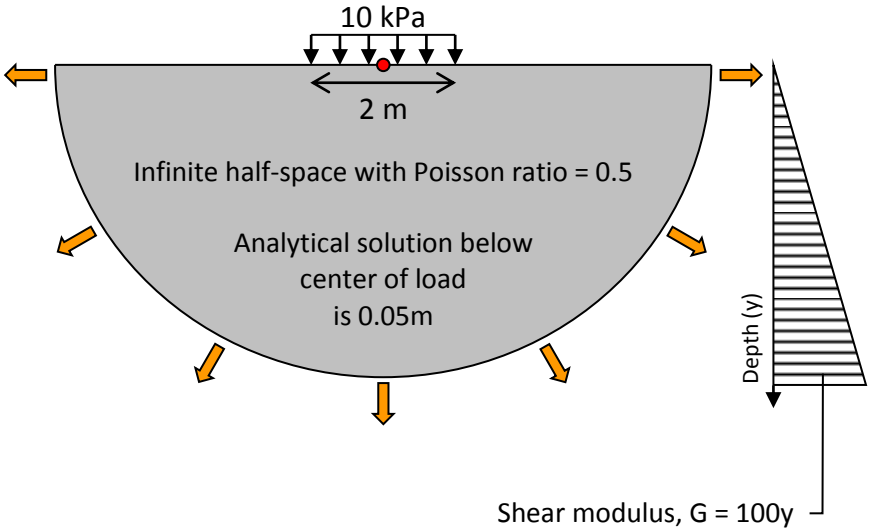


Figure 2-1 Flexible strip footing on an elastic Gibson soil

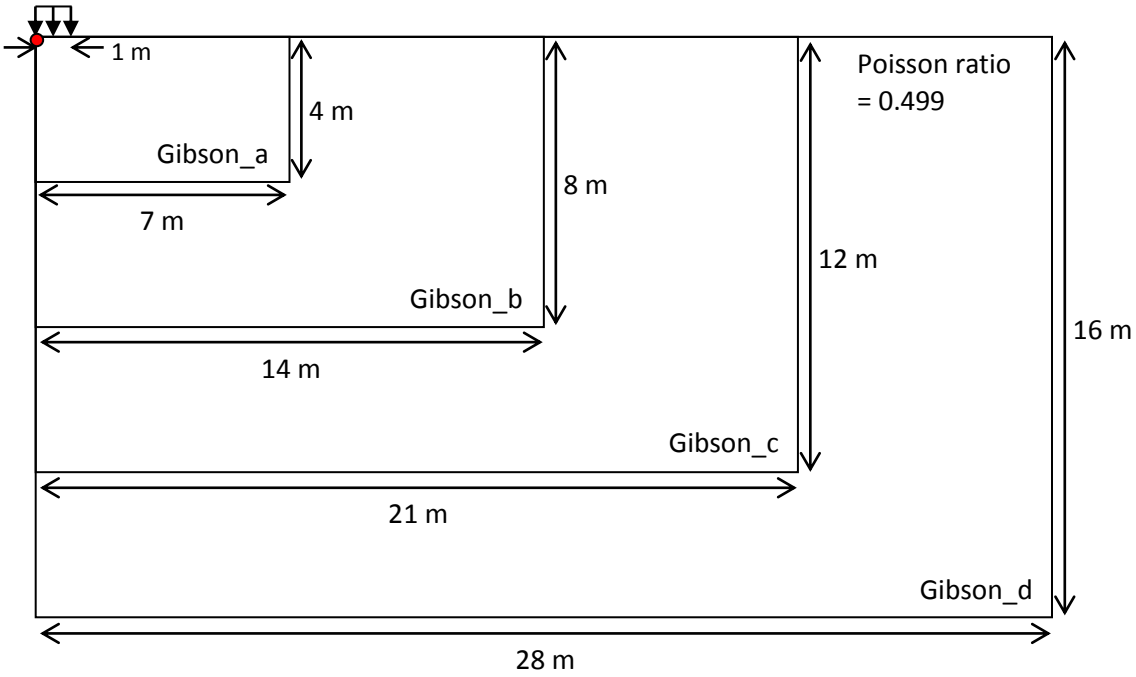


Figure 2-2 Problem domain sizes considered for finite element analyses

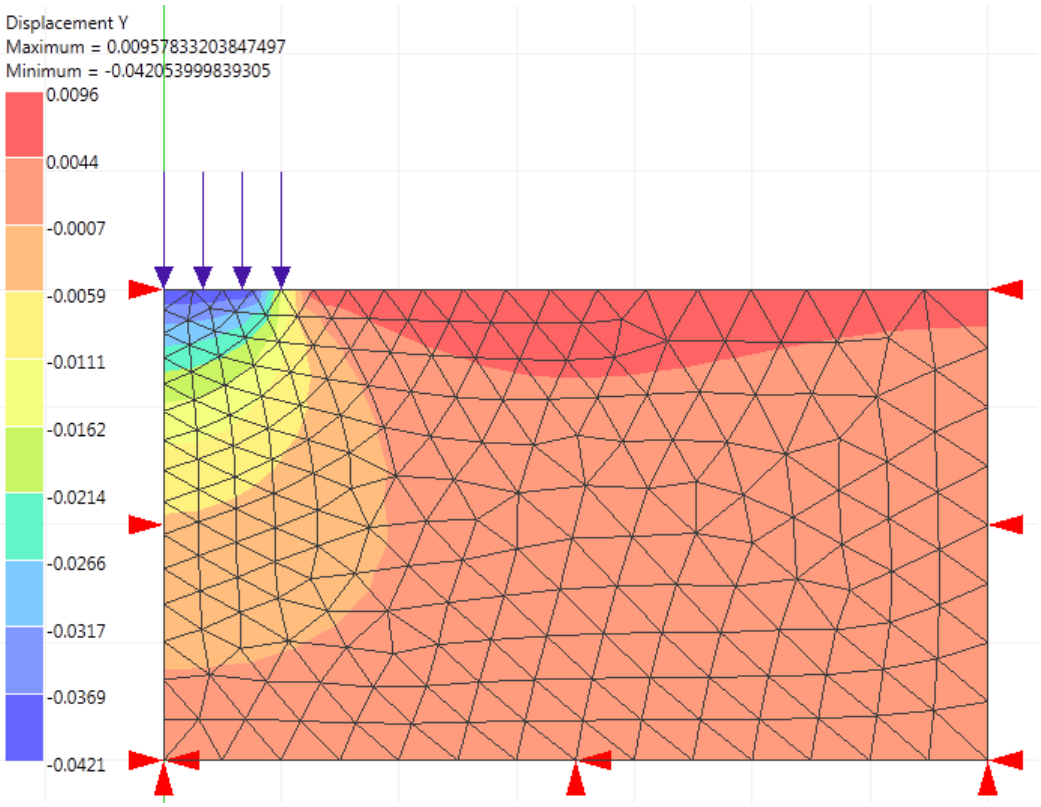


Figure 2-3 Vertical settlement from finite element analyses for Gibson_a – 7m×4m

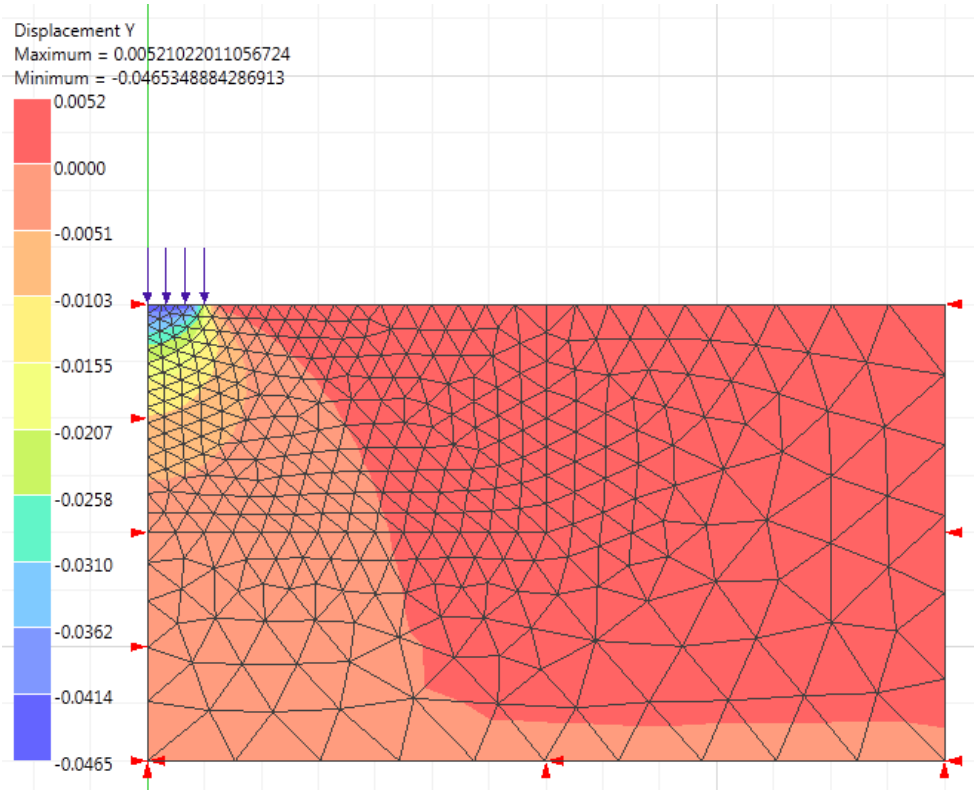


Figure 2-4 Vertical settlement from finite element analyses for Gibson_b – 14m×8m

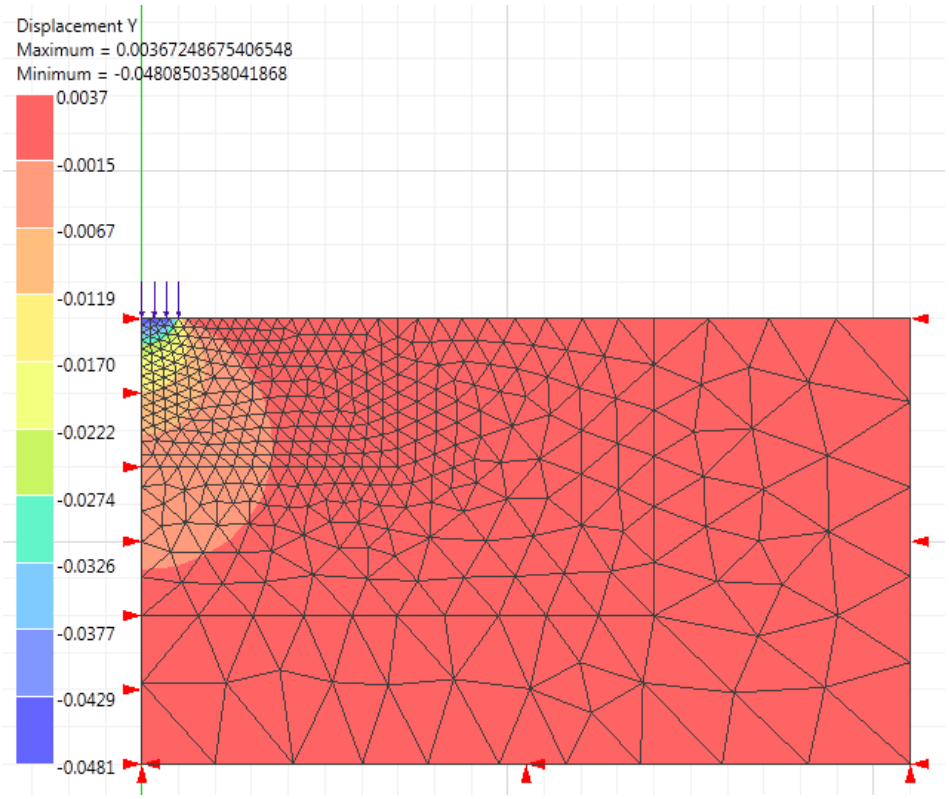


Figure 2-5 Vertical settlement from finite element analyses for Gibson_c – 21m×12m

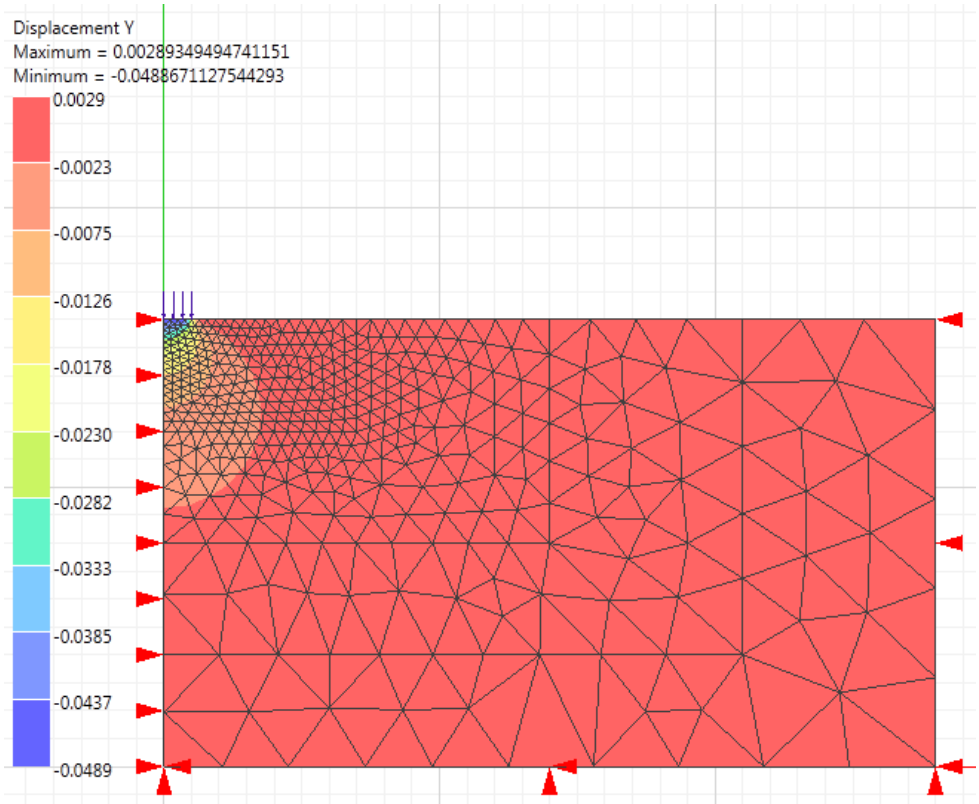


Figure 2-6 Vertical settlement from finite element analyses for Gibson_d – 28m×16m

The further the boundary of the mesh from the strip loading, the closer is the central settlement to the analytical solution of 0.05m. Since the soil layer is of finite thickness, the settlement obtained from the analyses should not exceed 0.05m. This problem also illustrates the importance of setting appropriate vertical and lateral extents of the finite element mesh. This will depend on the problem being analysed, the constitutive models employed and which facet of behaviour is under investigation.

***Reference***

[1] Gibson, R. E. Some Results Concerning Displacements and Stresses in a Non-Homogeneous Elastic Half-Space, Geotechnique 17(1), 58–67, 1967.

# 1-D consolidation

**To verify and validate:** consolidation, elastic model, linear strain triangle element, pore-pressure fixities, distributed line loading

When a soil layer is subjected to an external loading, immediately the water will alone sustain this load and cause the build-up the excessive pore water pressure. In the progress of the flow of the water to the surface, the load is gradually transferred to the soil skeleton and the excessive pore water pressure will dissipate. At the same time, the settlement of the soil layer occurs. As settlement is usually a major concern in geotechnical engineering, this is a key problem in soil mechanics.

Consider a soil layer composed of an isotropic, homogeneous and saturated thermoporoelastic material. The layer has a thickness of, h, in the y direction and of infinite extent in the two other directions x and z. The layer is underlain by a rigid and impervious base at y = 0. And the top surface at y = h is so perfectly drained that the pore pressure is held constant as zero.

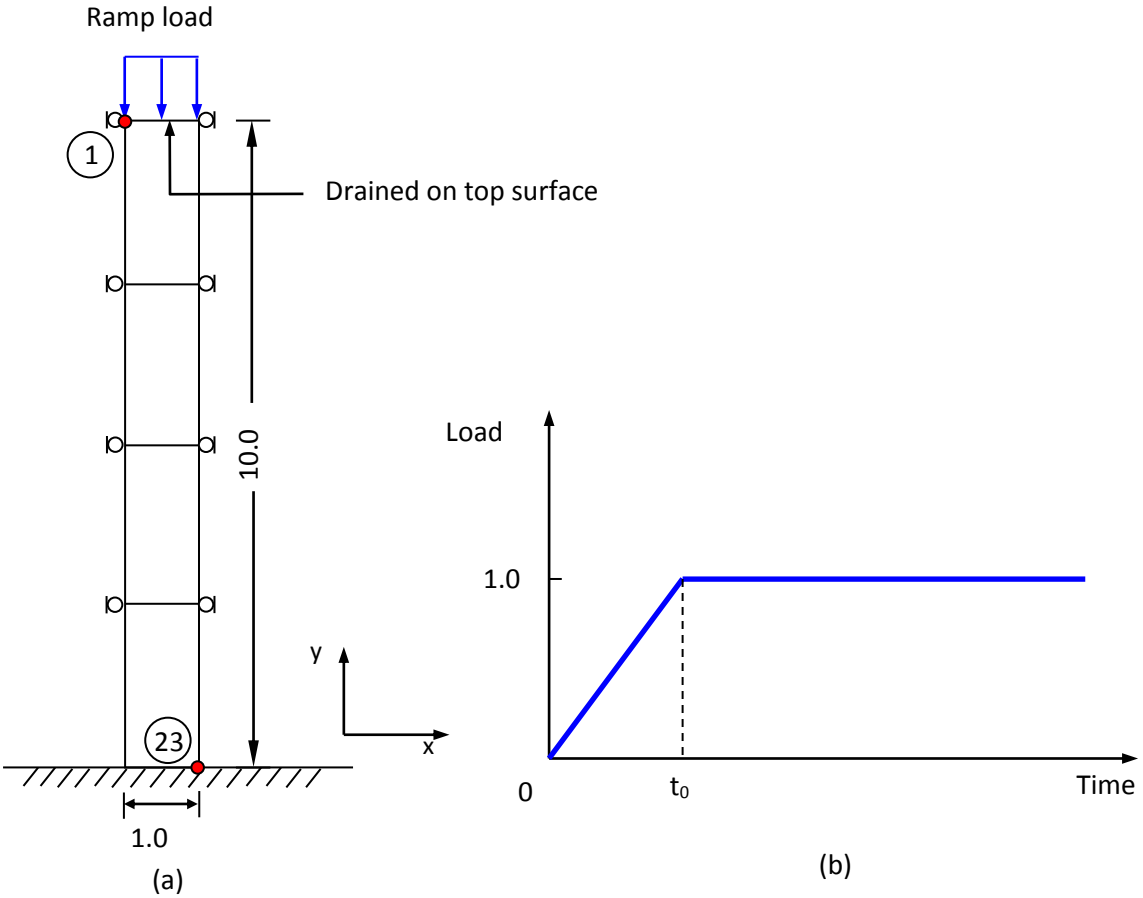


Figure 3-1 (a) Biot's consolidation of a rectangular solid in plane strain, (b) Ramp loading

The material properties, boundary and loading conditions are modelled after Smith & Griffiths (1997). A uniform vertical pressure of 1 kPa is applied on the top surface of the soil column as ramped loading. As the bottom of the soil column is modelled as

an undeformable and impermeable layer, both the solid and fluid displacements are fixed. The pore pressure is kept constant as zero at the top surface of the soil column because of the perfectly drained condition. For the reason of 1D consolidation problem, all the lateral movement of the solid and fluid phase are suppressed so that the vertical displacement is the only non-zero displacement for the intermediate nodes.

The height of the soil column is 10m. Smith & Griffiths (1997) have used four linear strain quadrilateral elements are used to model the horizontal layer. We used one hundred and eighty-five linear strain triangle finite elements to model the problem.

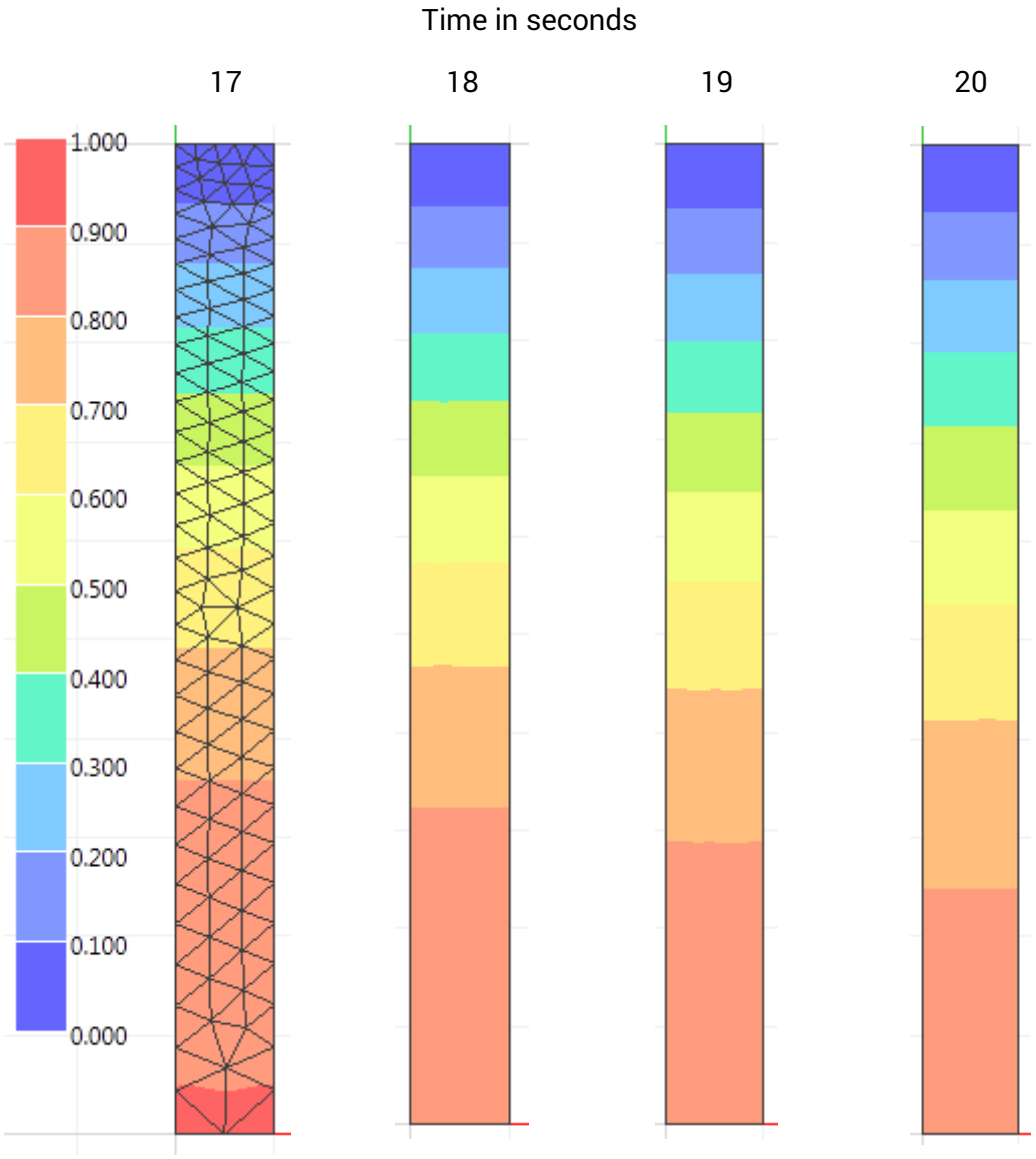


Figure 3-2 Contour of pore pressures at different time steps

Table 3-1 Comparison of displacement and pore pressures at top and bottom nodes of the mesh

| Time in seconds | Smith & Griffiths (1997) | GeoFEA 9.0 | Percentage difference |
|---|---|---|---|
| Displacements at node 1 | | | |
| 17 | -3.966 | -3.92093 | 1.14% |
| 18 | -4.125 | -4.08159 | 1.05% |
| 19 | -4.277 | -4.23565 | 0.97% |
| 20 | -4.424 | -4.38382 | 0.91% |
| Pore pressures at node 23 | | | |
| 17 | 0.9144 | 0.90186 | 1.37% |
| 18 | 0.8981 | 0.88605 | 1.34% |
| 19 | 0.8811 | 0.86964 | 1.30% |
| 20 | 0.8636 | 0.85278 | 1.25% |

***Reference***

[1] Smith IM, Griffiths DV. Programming the Finite Element Method (3rd edn), John Wiley: Chichester, 1997.

# Cryer's consolidation sphere

**To verify and validate:** consolidation, elastic model, pore-pressure fixities, distributed surface loading, axisymmetry, 3D tetrahedron

The consolidation of a fluid-saturated porous elastic sphere which is subjected to a uniform normal traction q applied to the surface, from which pore fluid can drain freely, was first considered by Cryer (1963). He showed that the pore fluid pressure in the interior of the sphere jumped by an amount q when the surface traction was applied and then continued to increase for some time before it decayed. This phenomenon, a rise in interior pore fluid pressure followed by dissipation, during the consolidation of a porous elastic body, is called the Mandel-Cryer effect.

The numerical analysis is conducted following the parameters used by Wong et. al. (1998):

Table 4-1 Parameters used for the finite element analysis

| | |
|---|---|
| Effective Young's modulus, E' | 10 000 kPa |
| Poisson Ratio, v | 0.0, 0.33, 0.49, respectively |
| unit weight of water, $\gamma_w$ | 10 kN/m$^3$ |
| Porous media's hydraulic conductivity, k | 4.91× 10-5 m/s |
| Radius of Cryer's sphere, a | 1 m |
| Surface pressure load, q | 100 kPa |
| Time, t (s) | — |

The Cryer's dimensionless time can be obtained as

$$T = \frac{C_v t}{a^2} = \frac{E' k (1-\nu) t}{(1+\nu)(1-2\nu)\gamma_w a^2}$$

where $C_v$ is consolidation coefficient.

Cryer (1963) did not investigate the time evolution of the other stress and strain components during the consolidation of a sphere. In order to obtain a complete understanding of the process of consolidation of a porous elastic sphere, Mason et al (1991) analyzed systematically the evolution of stress and strain during the consolidation. The analytical series solution for center pore water pressure was given in the paper by Mason et al (1991).

$$p(0,t) = 4(1-2\nu)(1-\nu)q\sum_{n=1}^{\infty}\frac{\left(\sin\sqrt{x_n} - \sqrt{x_n}\right)e^{-x_n t}}{\left[2(1+\nu)(1-2\nu) - (1-\nu)^2 x_n\right]\sin\sqrt{x_n}}$$

where

p : pressure of the fluid in the pores

t : consolidation time

v : Poisson's ratio

q : all-round pressure applied to the enveloped sphere

$x_n$ : contribution to the integral from the poles at non-zero root of the equation, $-x_n$, n = 1,2,3,... (n≠0)

MATLAB is used to calculate the analytical series solution and truncate the non-dominant terms in a summation of infinite terms. The total time, incremental time and square root of Cryer's dimensionless time throughout sequential stages, are tabulated as follows,

Table 4-2 Parameters used for the finite element analysis

| Stage | Total Time | Time increment | Cryer time, $\sqrt{T}$ | | |
|---|---|---|---|---|---|
| | | | ν=0.0 | ν=0.33 | ν=0.49 |
| 1(I) | 0.0000000 | - | - | - | - |
| 2(II) | 0.0000000 | Δt | - | - | - |
| 3(III) | 0.0033700 | 0.0033700 | 0.0128634 | 0.0156577 | 0.0532148 |
| 4 | 0.0067400 | 0.0033700 | 0.0181916 | 0.0221433 | 0.0752571 |
| 5 | 0.0115059 | 0.0047659 | 0.0237684 | 0.0289316 | 0.0983280 |
| 6 | 0.0162717 | 0.0047659 | 0.0282655 | 0.0344056 | 0.1169322 |
| 7 | 0.0230117 | 0.0067400 | 0.0336136 | 0.0409154 | 0.1390567 |
| 8 | 0.0297517 | 0.0067400 | 0.0382205 | 0.0465231 | 0.1581152 |
| 9 | 0.0392832 | 0.0095315 | 0.0439182 | 0.0534584 | 0.1816859 |
| 10 | 0.0488147 | 0.0095315 | 0.0489571 | 0.0595920 | 0.2025317 |
| 11 | 0.0622942 | 0.0134795 | 0.0553050 | 0.0673188 | 0.2287924 |
| 12 | 0.0757737 | 0.0134795 | 0.0609958 | 0.0742458 | 0.2523347 |
| 13 | 0.0948362 | 0.0190625 | 0.0682382 | 0.0830615 | 0.2822960 |
| 14 | 0.1138987 | 0.0190625 | 0.0747825 | 0.0910274 | 0.3093692 |
| 15 | 0.1408572 | 0.0269585 | 0.0831630 | 0.1012284 | 0.3440386 |
| 16 | 0.1678157 | 0.0269585 | 0.0907731 | 0.1104916 | 0.3755208 |
| 17 | 0.2059402 | 0.0381245 | 0.1005568 | 0.1224006 | 0.4159952 |
| 18 | 0.2440647 | 0.0381245 | 0.1094695 | 0.1332494 | 0.4528665 |
| 19 | 0.2979797 | 0.0539150 | 0.1209579 | 0.1472334 | 0.5003928 |
| 20 | 0.3518947 | 0.0539150 | 0.1314459 | 0.1599997 | 0.5437810 |
| 21 | 0.4281447 | 0.0762500 | 0.1449893 | 0.1764851 | 0.5998090 |
| 22 | 0.5043947 | 0.0762500 | 0.1573715 | 0.1915570 | 0.6510329 |
| 23 | 0.6122247 | 0.1078300 | 0.1733789 | 0.2110417 | 0.7172542 |
| 24 | 0.7200547 | 0.1078300 | 0.1880284 | 0.2288736 | 0.7778582 |
| 25 | 0.8725447 | 0.1524900 | 0.2069830 | 0.2519456 | 0.8562716 |
| 26 | 1.0250347 | 0.1524900 | 0.2243417 | 0.2730751 | 0.9280834 |
| 27 | 1.2406897 | 0.2156550 | 0.2468154 | 0.3004308 | 1.0210554 |
| 28 | 1.4563447 | 0.2156550 | 0.2674070 | 0.3254955 | 1.1062411 |
| 29 | 1.7613247 | 0.3049800 | 0.2940766 | 0.3579584 | 1.2165709 |
| 30 | 2.0663047 | 0.3049800 | 0.3185209 | 0.3877127 | 1.3176950 |
| 31 | 2.4976047 | 0.4313000 | 0.3501891 | 0.4262601 | 1.4487036 |
| 32 | 2.9289047 | 0.4313000 | 0.3792219 | 0.4615997 | 1.5688099 |
| 33 | 3.5388547 | 0.6099500 | 0.4168426 | 0.5073927 | 1.7244439 |
| 34 | 4.1488047 | 0.6099500 | 0.4513384 | 0.5493819 | 1.8671500 |

| Stage | Total Time | Time increment | Cryer time, $\sqrt{T}$ | | |
|---|---|---|---|---|---|
| | | | ν=0.0 | ν=0.33 | ν=0.49 |
| 35 | 4.8988047 | 0.7500000 | 0.4904399 | 0.5969775 | 2.0289099 |
| 36 | 5.6488047 | 0.7500000 | 0.5266463 | 0.6410489 | 2.1786927 |
| 37 | 6.3988047 | 0.7500000 | 0.5605188 | 0.6822795 | 2.3188205 |
| 38 | 7.1488047 | 0.7500000 | 0.5924579 | 0.7211566 | 2.4509498 |
| 39 | 7.8988047 | 0.7500000 | 0.6227610 | 0.7580425 | 2.5763116 |
| 40 | 8.6488047 | 0.7500000 | 0.6516566 | 0.7932150 | 2.6958501 |
| 41 | 9.3988047 | 0.7500000 | 0.6793242 | 0.8268927 | 2.8103086 |
| 42 | 10.1488047 | 0.7500000 | 0.7059081 | 0.8592515 | 2.9202844 |
| 43 | 10.8988047 | 0.7500000 | 0.7315267 | 0.8904352 | 3.0262662 |
| 44 | 11.6488047 | 0.7500000 | 0.7562779 | 0.9205631 | 3.1286601 |
| 45 | 12.3988047 | 0.7500000 | 0.7802444 | 0.9497357 | 3.2278074 |
| 46 | 13.1488047 | 0.7500000 | 0.8034963 | 0.9780386 | 3.3239987 |
| 47 | 13.8988047 | 0.7500000 | 0.8260940 | 1.0055452 | 3.4174835 |
| 48 | 14.6488047 | 0.7500000 | 0.8480898 | 1.0323191 | 3.5084783 |

## Axisymmetry modeling of Cryer's consolidation problem

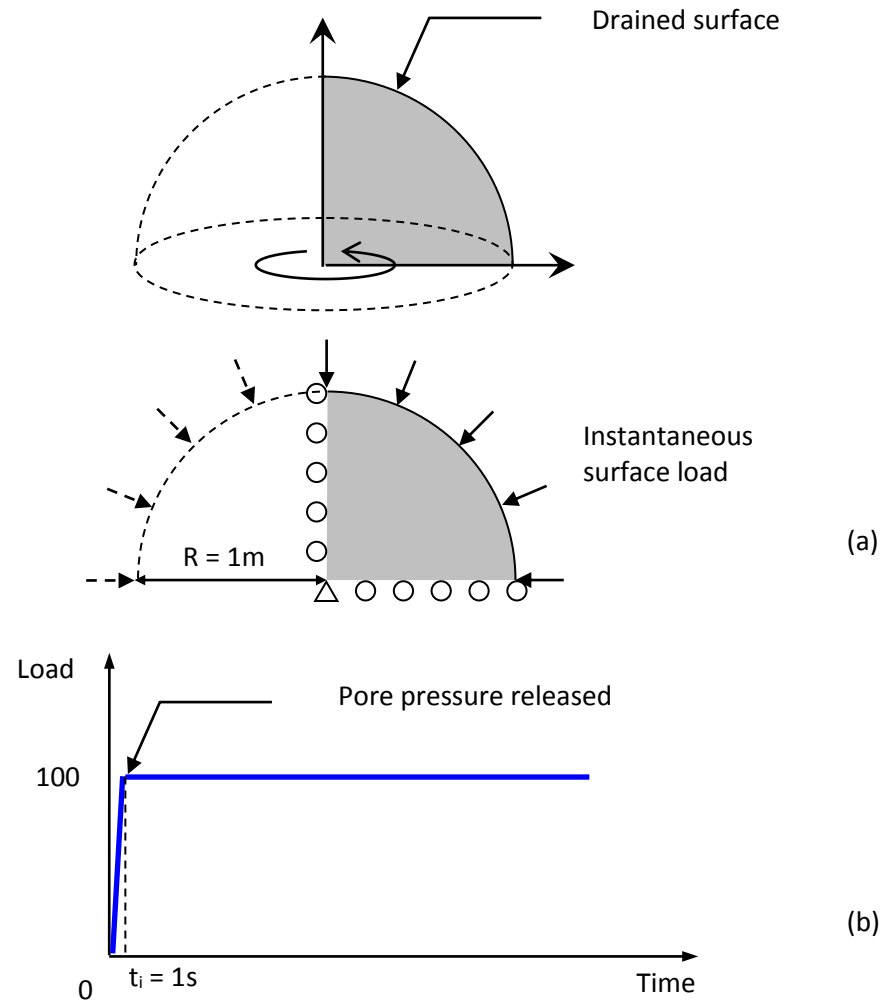


Figure 4-1 (a) Schematic description of the Cryer's consolidation problem in axisymmetric analysis, (b) Ramp loading

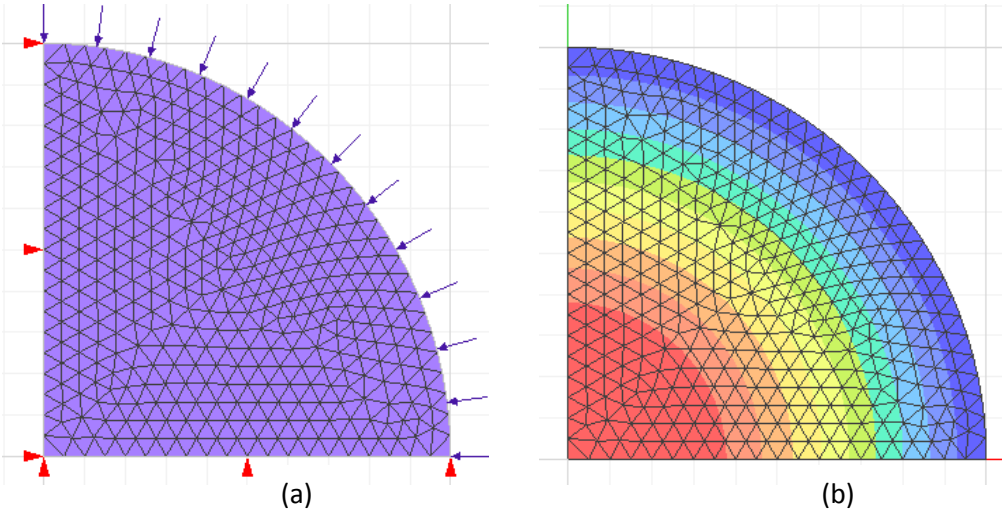


Figure 4-2 (a) Finite element mesh used for the axisymmetric analysis, (b) Counter of excess pore pressures

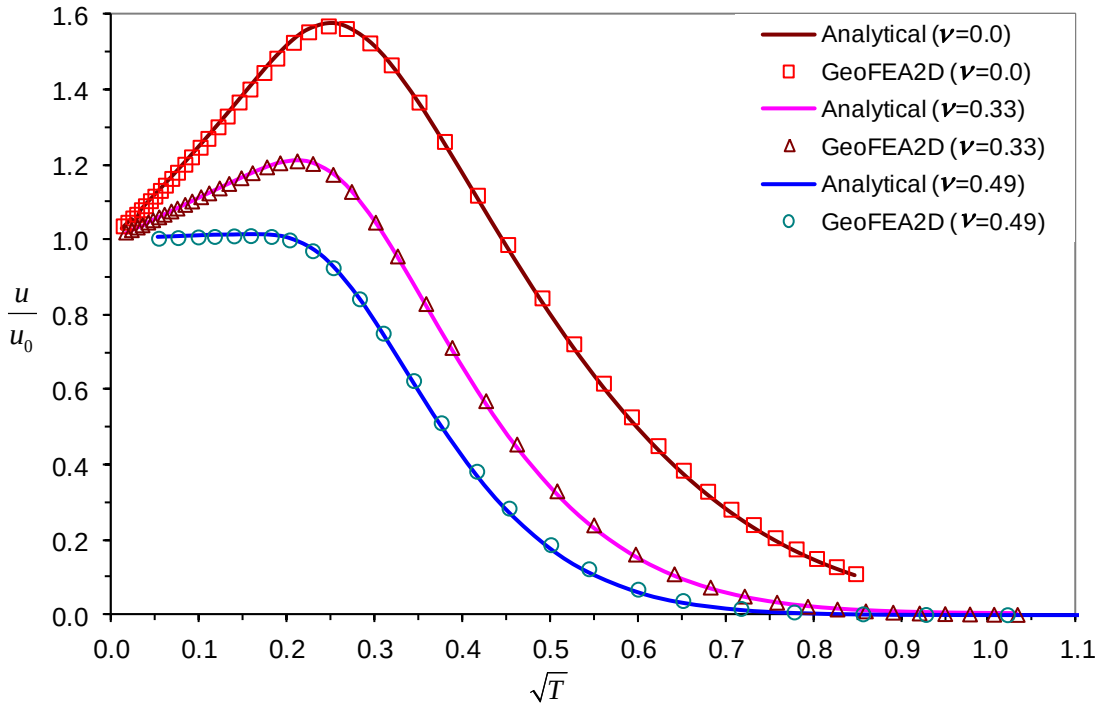


Figure 4-3 Numerical results (axisymmetric) of excess pore pressures versus analytical solutions at different Poisson's ratios

## 3-D modeling of Cryer's consolidation problem

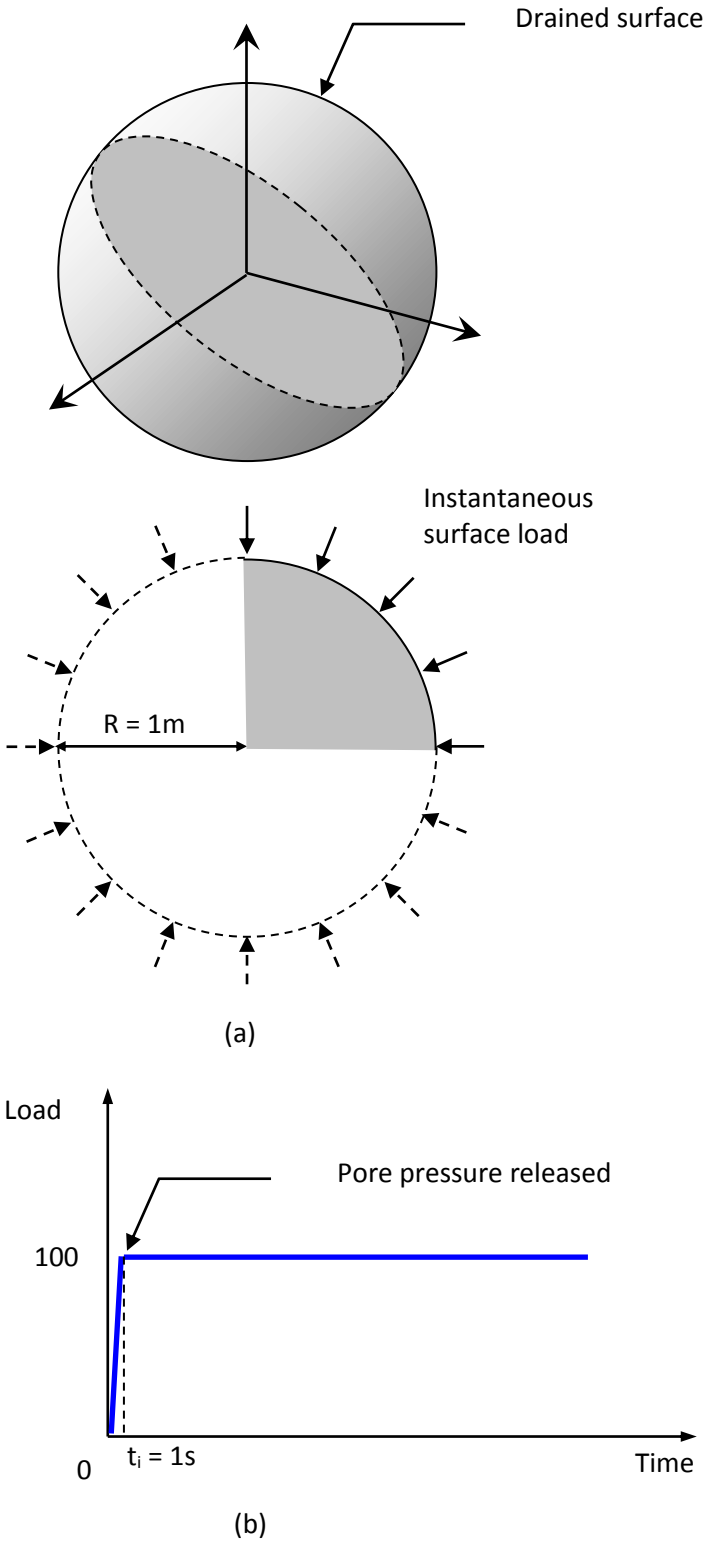


Figure 0-4 (a) Schematic description of Cryer's consolidation in 3-dimensional space, (b) Ramp loading

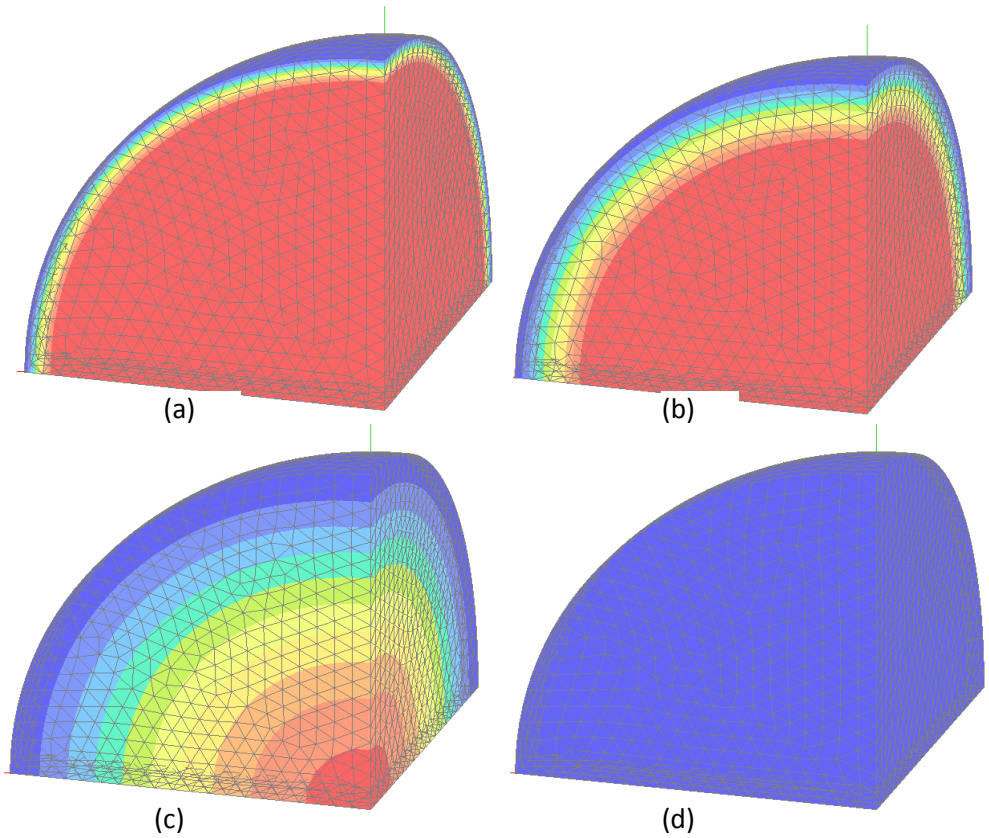


Figure 4-5 Counters of excess pore pressures at different time steps: (a) at stage 10, (b) at stage 20, (c) at stage 30, (d) at stage 40 out of total 47 stages of the analysis

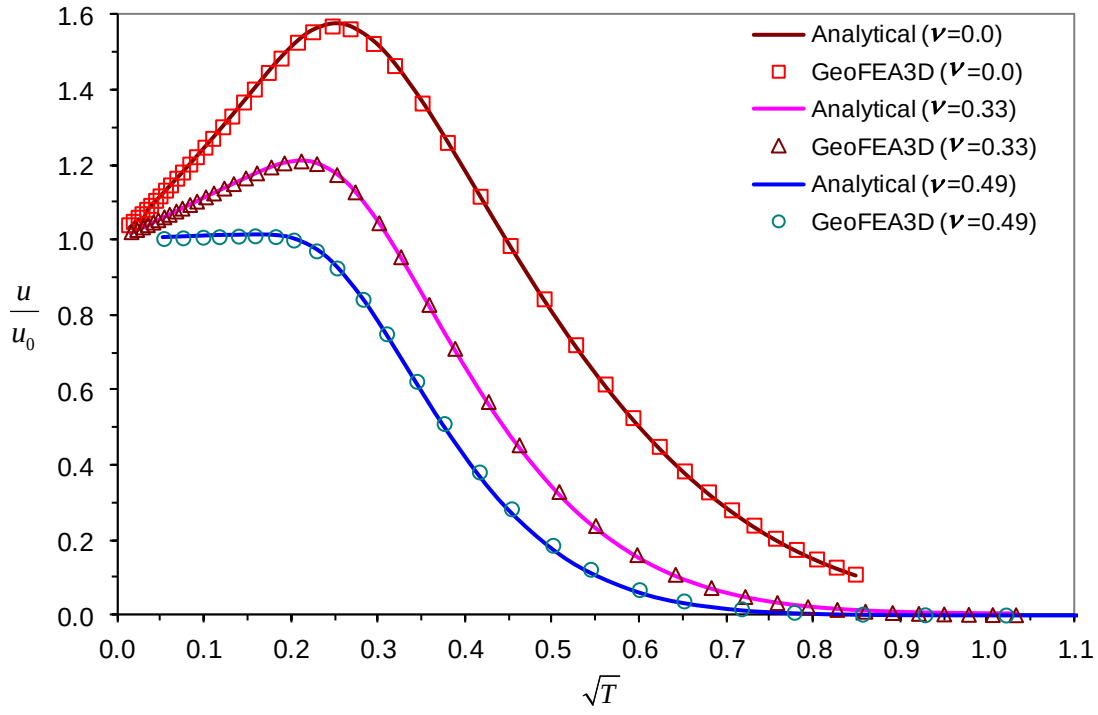


Figure 4-6 Numerical results (3-D) of excess pore pressures versus analytical solutions at different Poisson's ratios

***Reference***

[1] Cryer CW. A comparison of the three-dimensional consolidation theories of Biot and Terzaghi. Quarterly Journal of Mechanics and Applied Mathematics, 1963; 16:401-412.
[2] Mason, DP, Solomon A, Nicolaysen LO. Evolution of stress and strain during the consolidation of a fluid-saturated porous elastic sphere, Journal of Applied Physics, 1991; 70(9):4724-4740.
[3] Wong TT, Fredlund DG, Krahn J. A numerical study of coupled consolidation in unsaturated soils, Canadian Geotechnical Journal, 1998; 35(6): 926-937.

# Cylindrical Hole in an Infinite Space Using Mohr-Coulomb Material

**To verify and validate:** associated and non-associated flow Mohr-Coulomb model

The problem deals with the determination of stresses and displacements for the case of a cylindrical hole in an infinite elasto-plastic medium subjected to in-situ stresses. In the two numerical simulations, the far boundaries are situated at a distance of ten and twenty hole-diameters from the axis of the hole. The radius, a (a = 1.0 m), of the hole is small enough if compared to the length of the cylinder, so that plane-strain conditions are applicable. The initial stress state (corresponding to $P_0$ = 30 MPa) is applied throughout the domain, the pressure inside the hole required in the closed-form solution is neglected as the hole is created. The solution chosen for presentation was obtained and used to validate the associated and non-associated flow Mohr-Coulomb yield condition that was added to the finite element code.

The Mohr-Coulomb material is assigned with the following properties:

| | | |
|---|---|---|
| Modulus of elasticity | : | E = 6.78 GPa |
| Poisson's ratio | : | K = 0.21 |
| Cohesion | : | c = 3.45 MPa |
| Friction angle | : | $\phi$ = 30° |
| Dilation angles | : | $\psi$ = 0° and 30° |

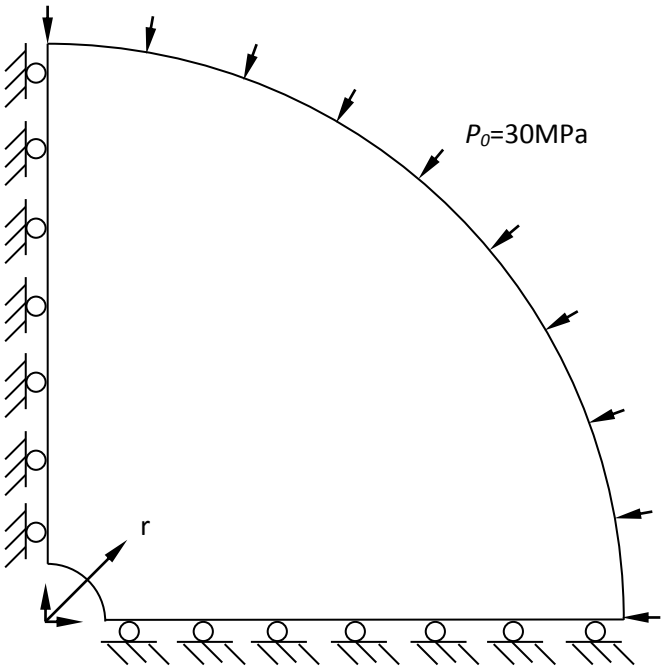


Figure 5-1 Problem description of a cylindrical hole in an infinite space

The analytical solution for this problem may be found in Salençon (1969) and Yu (2000). The yield zone radius, $R_0$, can be expressed as

$$\frac{R_0}{a} = \left[ \frac{2}{K_p + 1} \frac{1 + \frac{q}{P_0} k_p}{\frac{P_i}{P_0} + \frac{q}{P_0} k_p} \right]^{kp}$$

In which a is the hole radius, $P_0$ is the absolute value of the in-situ isotropic stress, $P_i$ is the pressure inside the hole (in our case, 0 MPa), and

$$K_p = \frac{1+\sin\varphi}{1-\sin\varphi} \; K_p = \frac{1 + sin\emptyset}{1 - sin\emptyset}$$

$$k_p = \frac{1}{K_p - 1}$$

$$q = 2 \cdot c \cdot \sqrt{K_p}$$

The radial stress at the elastic/plastic interface is

$$\frac{\sigma_{re}}{P_0} = -\frac{1}{K_p + 1}\left(2 - \frac{q}{P_0}\right)$$

The stresses in the plastic zone have the form

$$\frac{\sigma_r}{P_0} = \frac{q}{P_0} k_p - \left(\frac{P_i}{P_0} + \frac{q}{P_0} k_p\right)\left(\frac{r}{a}\right)^{K_p - 1}$$

$$\frac{\sigma_\theta}{P_0} = \frac{q}{P_0} k_p - K_p\left(\frac{P_i}{P_0} + \frac{q}{P_0} k_p\right)\left(\frac{r}{a}\right)^{K_p - 1}$$

In which r is the distance from the hole's axis. The stresses in the elastic zone are

$$\frac{\sigma_r}{P_0} = -1 - \frac{(1 - K_p) - \frac{2c\cos\varphi}{P_0(1-\sin\varphi)}}{1 + K_p}\left(\frac{R_0}{r}\right)^2$$

$$\frac{\sigma_\theta}{P_0} = -1 + \frac{(1 - K_p) - \frac{2c\cos\varphi}{P_0(1-\sin\varphi)}}{1 + K_p}\left(\frac{R_0}{r}\right)^2$$

The displacements in the elastic region, $u_r$, are given as

$$\frac{u_r}{a} = -\frac{(1 - K_p)P_0 - \frac{2c\cos\varphi}{(1-\sin\varphi)}}{2G(1 + K_p)}\left(\frac{R_0}{r}\right)^2\left(\frac{r}{a}\right)$$

In the plastic region, as

$$\frac{u_r}{a} = -\frac{P_0}{2G}\left(\frac{r}{a}\right)\left[\chi\left(\frac{r}{a}\right)\right]$$

In which

$$\left[\chi\left(\frac{r}{a}\right)\right] = (2\nu - 1)\left(1 + \frac{q}{P_0}k_p\right) + \frac{(1-\nu)\left(K_p^2 - 1\right)}{K_p + K_{ps}}\left(\frac{P_i}{P_0} + \frac{q}{P_0}k_p\right)\left(\frac{R_0}{a}\right)^{K_p - 1}\left(\frac{R_0}{r}\right)^{K_{ps}+1} + \left[(1-\nu)\frac{K_p K_{ps} + 1}{K_p + K_{ps}} - \nu\right]\left(\frac{P_i}{P_0} + \frac{q}{P_0}k_p\right)\left(\frac{r}{a}\right)^{K_p - 1}$$

And

$$K_{ps} = \frac{1 + \sin\psi}{1 - \sin\psi}$$

In these equations, υ is Poisson's ratio, ψ is the dilation angle, and G is the shear modulus.

The problem is modeled as two-dimensional plane-strain calculation using quarter symmetry. The boundary conditions applied to the model are shown below.

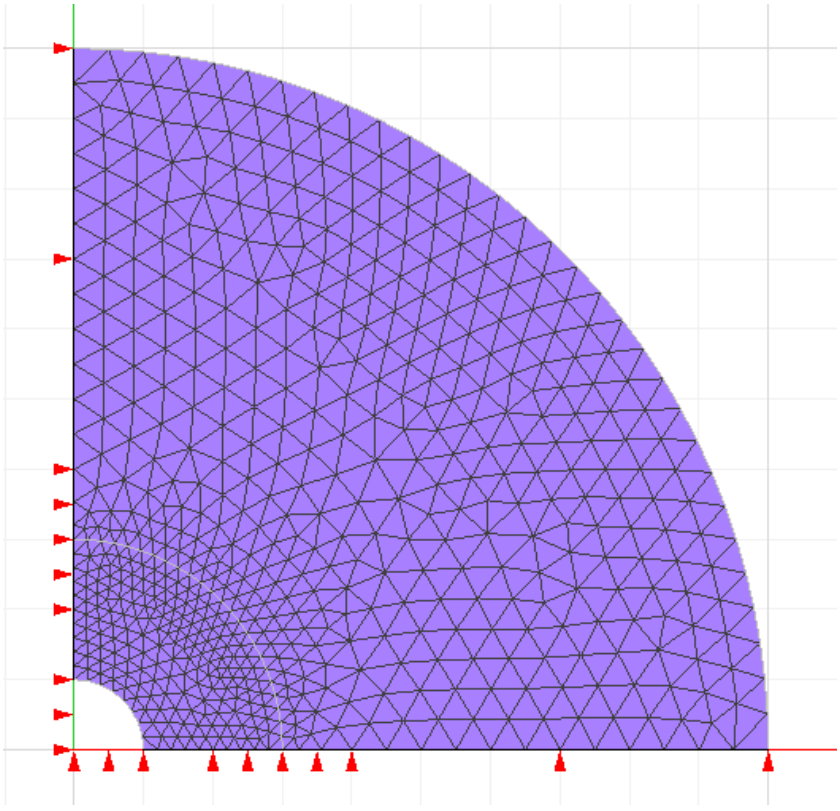

Figure 5-2 Finite element mesh used in the plane strain analysis

The following figures show the comparisons between GeoFEA results and the analytic solution along a radial line. Normalized stresses, $-\sigma_r/P_0$, $-\sigma_\theta/P_0$, and normalized displacements,$-u_r/a$ are plotted against normalized radius, r/a.

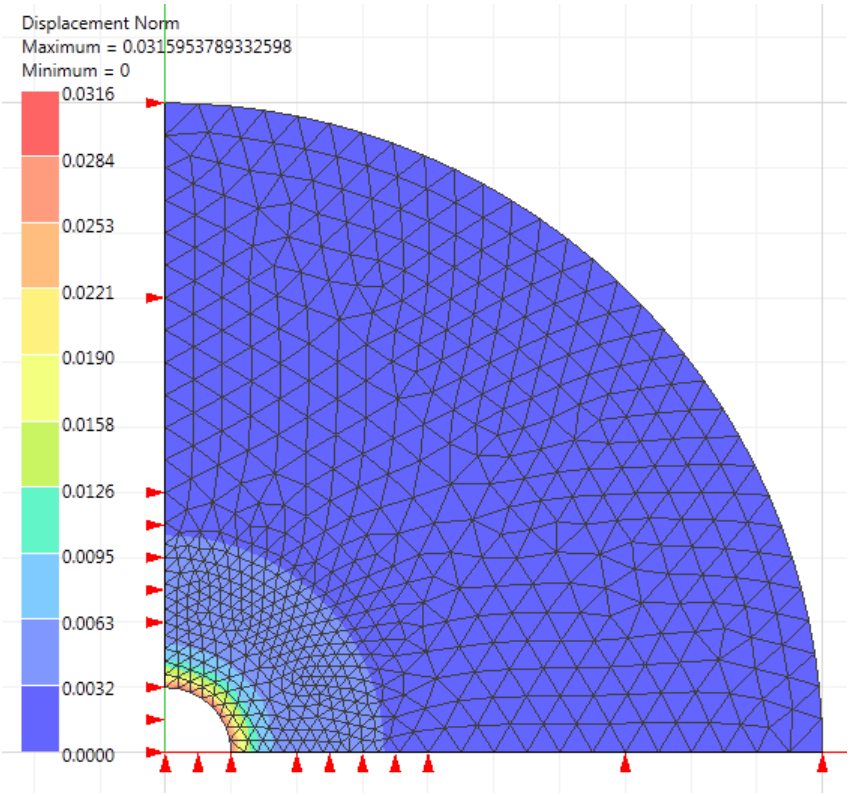


Figure 5-3 Contour of displacement norm after the hole is constructed - associated flow model (Radius, r = 10m)

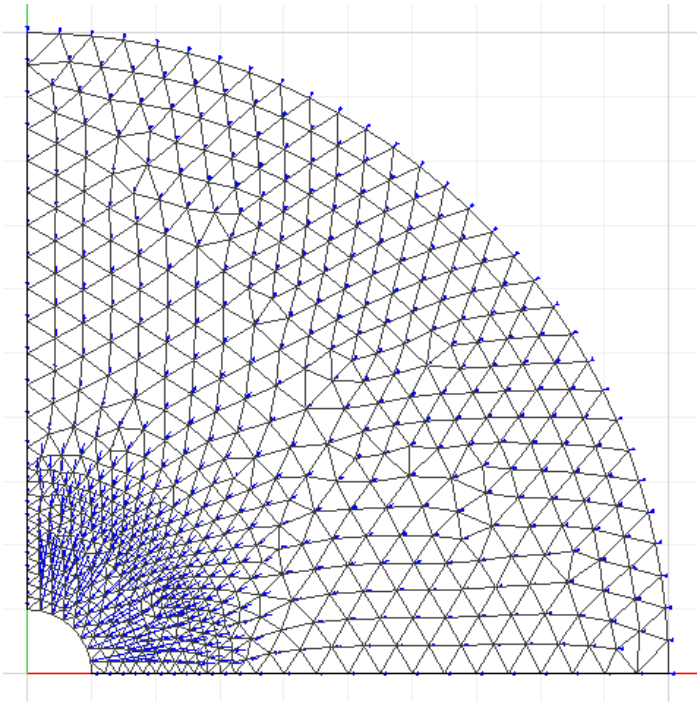

Figure 5-4 Displacement vectors - associated flow model (Radius, r = 10m)

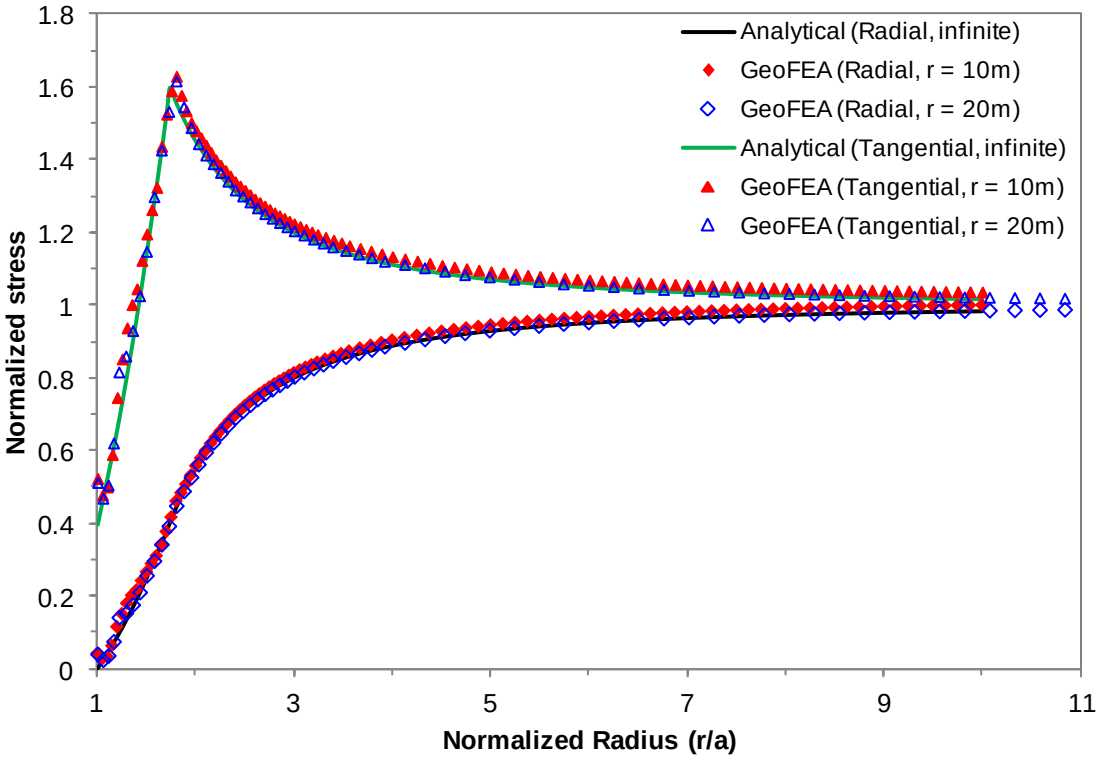


Figure 5-5 Stress comparison - associated flow ($\phi$ = 30°, $\psi$ = 30°)

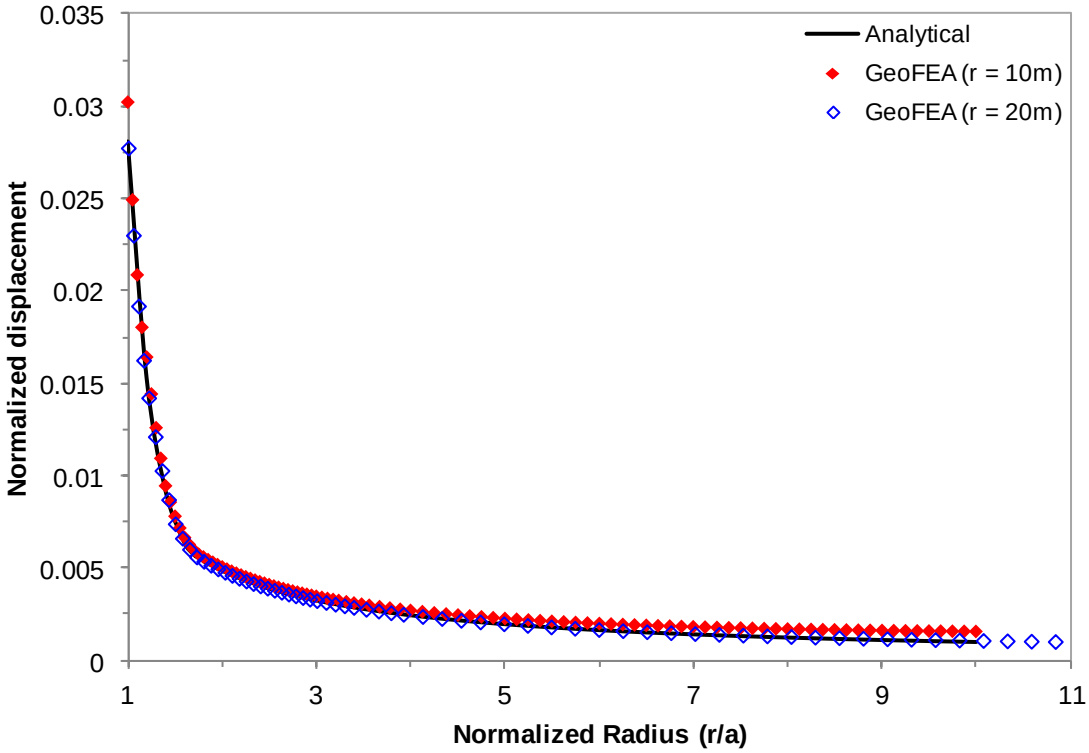


Figure 5-6 Displacement comparison - associated flow ($\phi$ = 30°, $\psi$ = 30°)

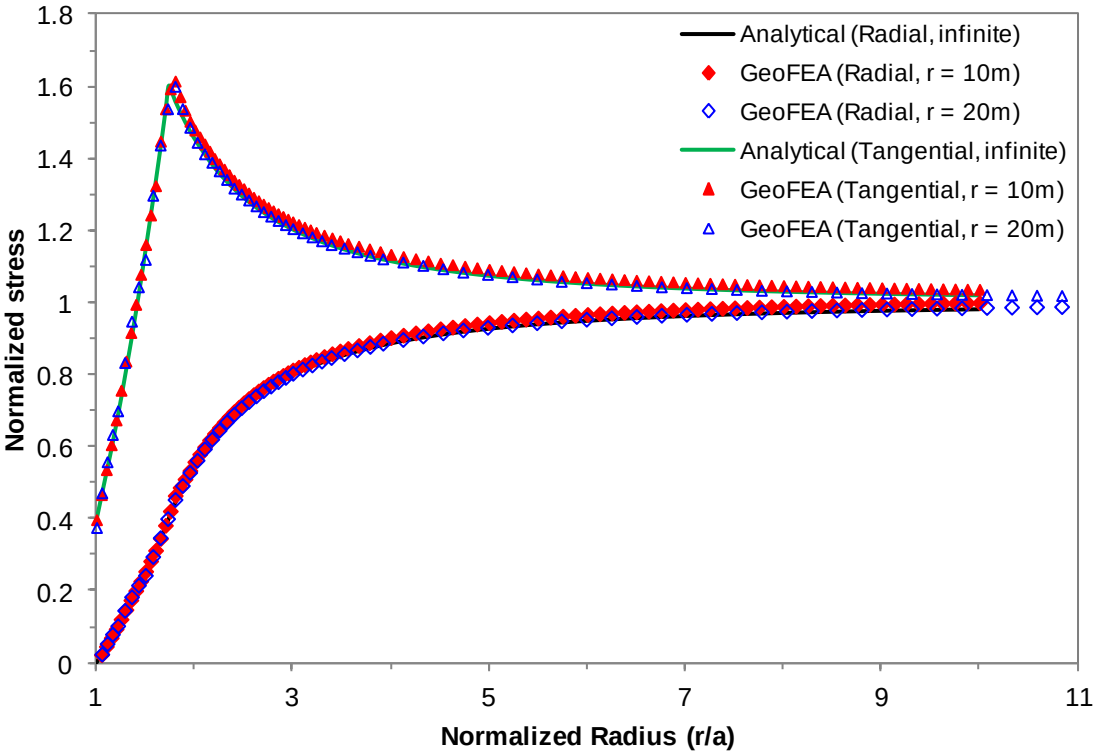


Figure 5-7 Stress comparison - non-associated flow ($\phi$ = 30°, $\psi$ = 0°)

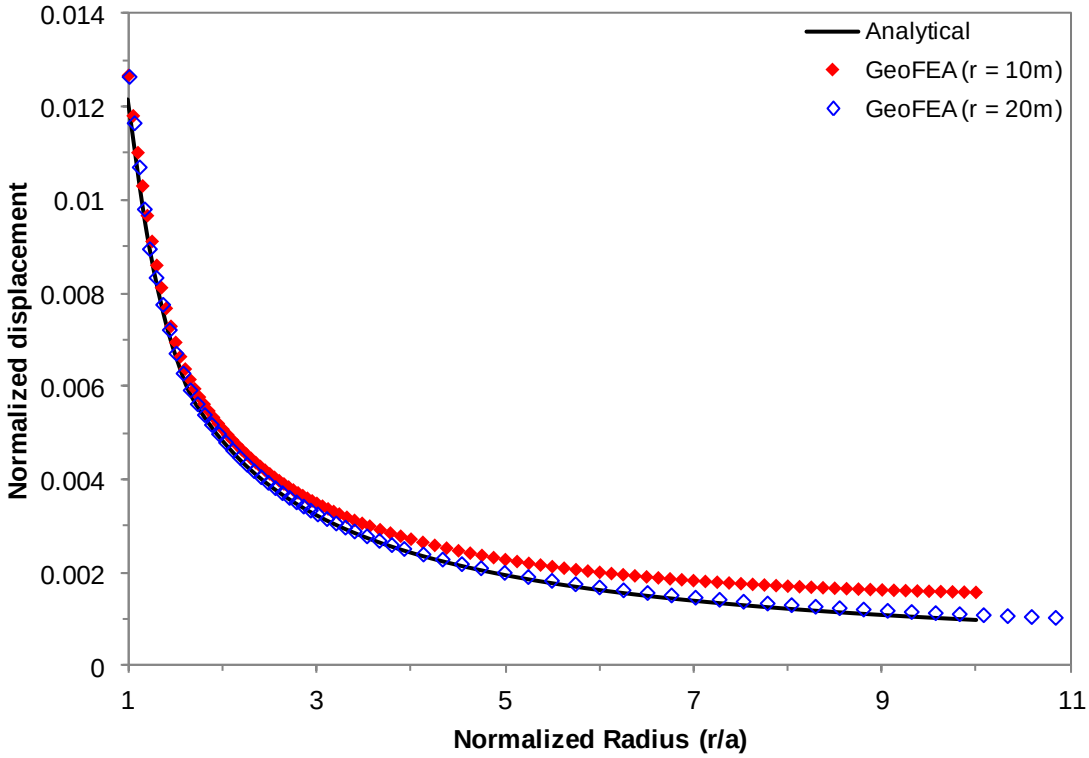


Figure 5-8 Displacement comparison - non-associated flow ($\phi$ = 30°, $\psi$ = 0°)

The significance of distance of far boundary away from the hole is clearly illustrated in the two simulations. The displacement at the hole approaches to the analytical solutions as the radius, r, is increased from 10m to 20m. The additional medium beyond the 10m boundary provided the additional buffer for the stress transition from the original 30MPa specific as the initial condition.

***Reference***


[1] Salençon J. Contraction Quasi-Statique D'une Cavite a Symetrie Spherique Ou Cylindrique Dans Un Milieu Elasto-Plastique, Annales Des Ports Et Chaussees, Vol. 4, 1969, 231-236.

[2] Yu H.S. Cavity Expansion Methods in Geomechanics, Kluwer Academic Publishers, 2000.

# Triaxial Compression Test on a Cam-Clay Sample

**To verify and validate:** Modified Cam-Clay model, drained and undrained analyses

Conventional drained and undrained triaxial compression tests on Cam-clay soil samples are modeled. The stresses and specific volume at the critical state are compared with analytical predictions. The responses of both lightly (LOC) and heavily (HOC) over-consolidated specimen are considered. This set of problems tests the prediction accuracy of the modified Cam-clay model in GeoFEA. The model of the sample is a cube with unit dimensions. The following properties of a Cam-clay material are assigned to the sample:

| | | |
|---|---|---|
| Frictional constant | : | M = 1.02 |
| Slope of normal consolidation line | : | λ = 0.2 |
| Slope of elastic swelling line | : | k = 0.05 |
| Poisson's ratio | : | υ = 0.145 |
| Reference pressure | : | $P_1'$ = 1 kPa |
| Pre-consolidation pressure | : | $P_{c0}'$ = 8×$P_1'$ and 40×$P_1'$ |
| Critical state void ratio at P1' | : | $e_{cs}$ = 2.216 |

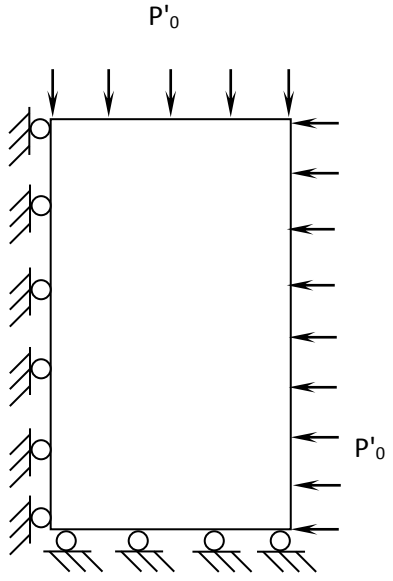


Figure 0-1 Isotropic compression of the soil sample at initial stage

Initially, the sample is in a state of isotropic compression corresponding to $P_0$ = 5$P_1'$and zero excess pore pressure ($P_0'$ = $P_0$). The pre-consolidation pressure, $P_{c0}$, has magnitude of 8×$P_1'$ for the lightly over-consolidated case and 40×$P_1'$ for the heavily

over-consolidated case. These cases correspond to an over-consolidation ratio R = $P_{c0}/P_0'$ of 1.6 and 8 respectively. The Poisson's ratio is assumed to remain constant during the test carried out with constant confining pressure $P_0$ and simulated strain-controlled platens. Drained and undrained tests are considered. Refer to Wood (1990) for a detailed discussion on the Cam-clay plasticity theory.

In a triaxial test:

$$\sigma_x = \sigma_z = \sigma_2$$

$$\sigma_y = \sigma_1$$

$$\tau_{xy} = \tau_{yz} = \tau_{zx} = 0$$

In which $\sigma_1$ is the axial stress and $\sigma_2$ is the cell pressure.

The mean pressure, p, and deviator stress, q, in a conventional triaxial test can be expressed as follows.

$$p = \frac{1}{3}\left(\sigma_1 + 2\sigma_2\right)$$

$$q = \left(\sigma_1 - \sigma_2\right)$$

Since the cell pressure is kept constant during the process of testing, the total stress path in the (p, q) plane is

$$\Delta q = 3\Delta p$$

## Drained test

In drained test, no excess pore pressure is generated, the effective and the total stress paths coincide, so

$$p' = \frac{q}{3} + P_0'$$

Numerical values for p' and q at the end of the simulation are compared with the analytical predictions. The results are presented in

Table 6-1.

Table 6-1 Comparison of numerical and analytical values of stresses at failure

| | OCR = 1.6 | OCR = 8 | Analytical |
|---|---|---|---|
| p | 7.573 | 7.617 | 7.576 |
| q | 7.719 | 7.846 | 7.727 |

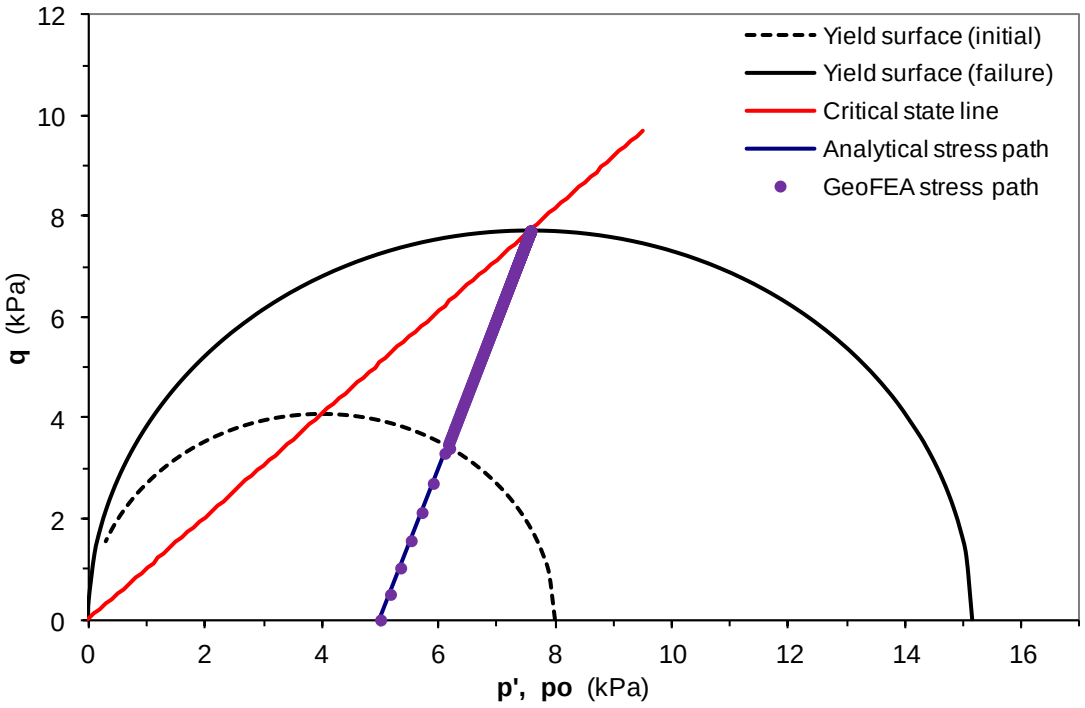


Figure 6-2 Effective stress path in stress space for drained test (OCR = 1.6)

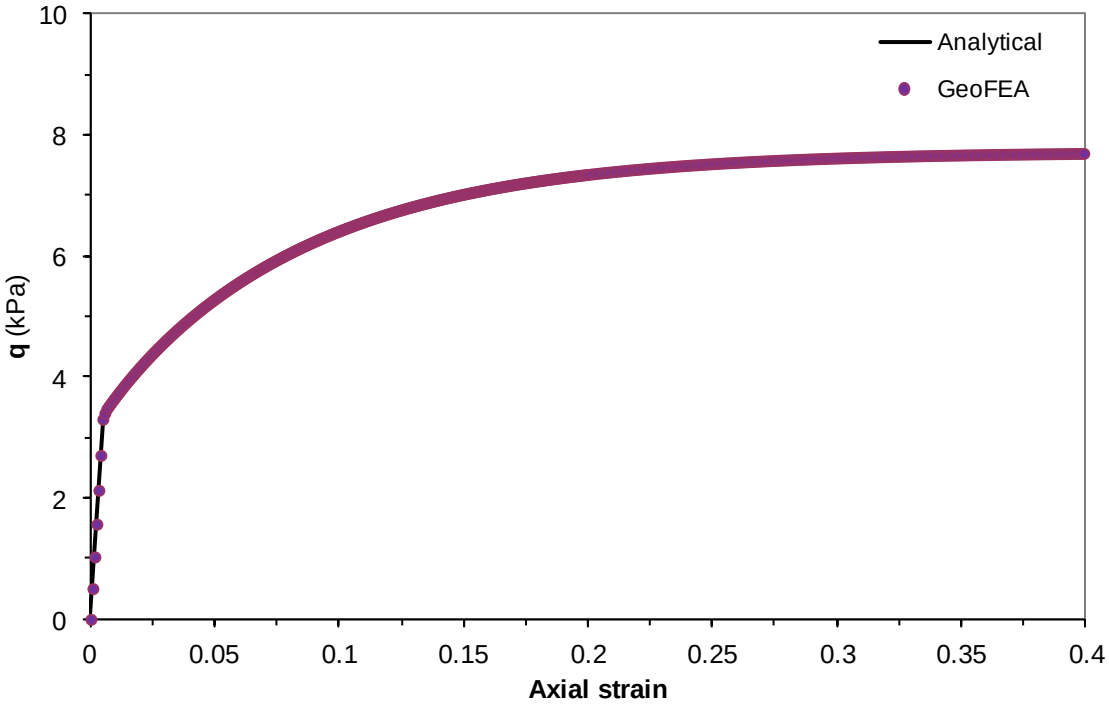


Figure 6-3 Relation between deviator stress and axial strain for drained test (OCR = 1.6)

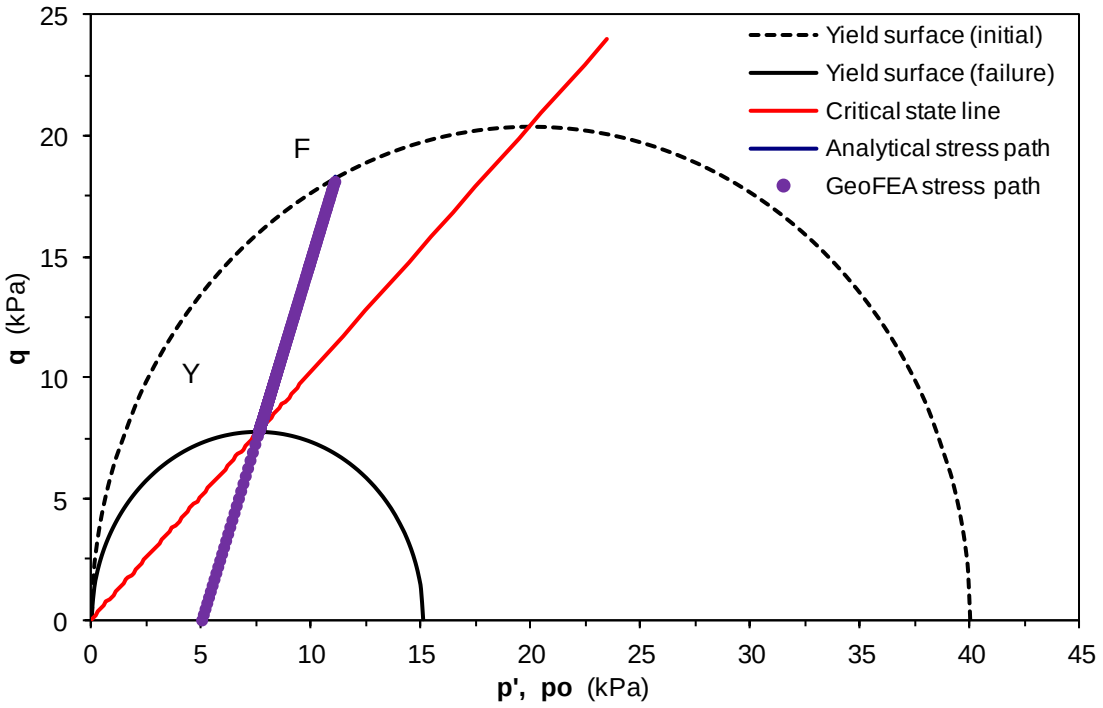


Figure 6-4 Effective stress path in stress space for drained test (OCR = 8.0)

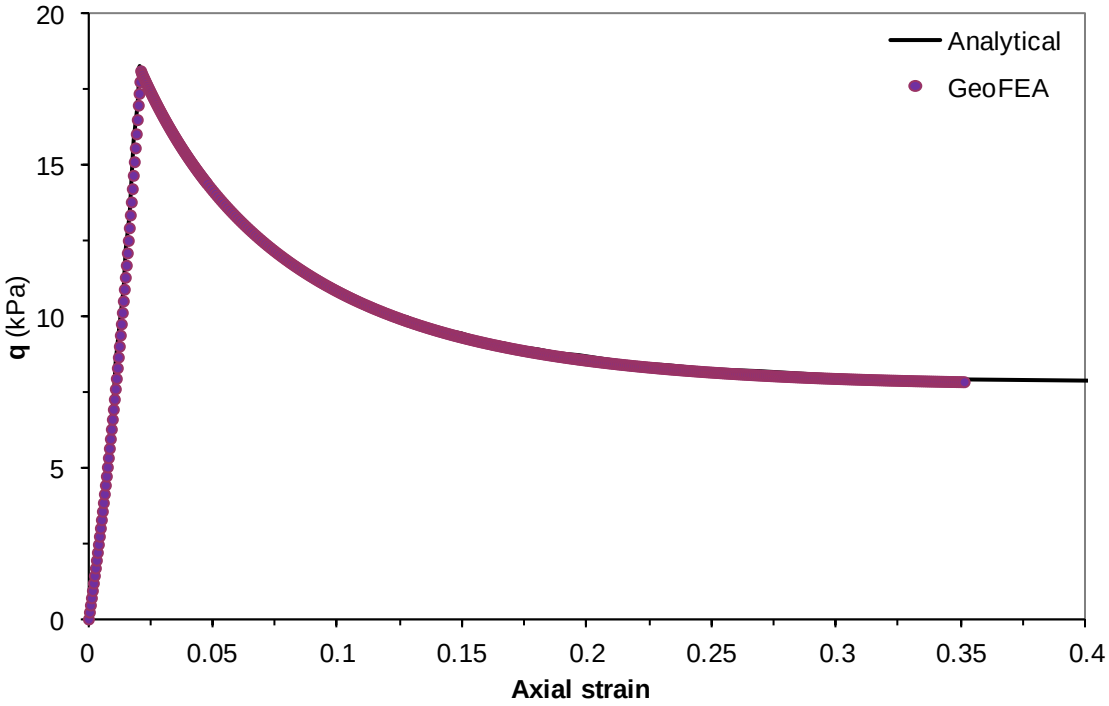


Figure 6-5 Relation between deviator stress and axial strain for drained test (OCR = 8.0)

## Undrained test

In an undrained test, which the fluid bulk modulus is much larger than that of the soil because the fluid is incompressible, the specific volume V remains constant, equal to the initial value $V_0$.

As long as the stress state lies inside the first yield surface, the path corresponds to the straight line,

$$p' = P_0'$$

The excess pore pressure u is given by

$$u = P - P'$$

$$u = \frac{q}{3} + P_0' - P'$$

And, at the critical state,

$$u_{cr} = \frac{q_{cr}}{3} + P_0' - P_{cr}'$$

Numerical values for p', q, and u at the end of the simulation are compared with the analytical predictions. The results are as presented in Table 6-2.

Table 6-2 Comparison of numerical and analytical values of stresses and pore pressure at failure

| | OCR = 1.6 | | OCR = 8.0 | |
|---|---|---|---|---|
| | Numerical | Analytical | Numerical | Analytical |
| p' | 4.200 | 4.229 | 13.982 | 14.142 |
| q | 4.284 | 4.314 | 14.343 | 14.425 |
| u | 2.228 | 2.209 | -4.202 | -4.334 |

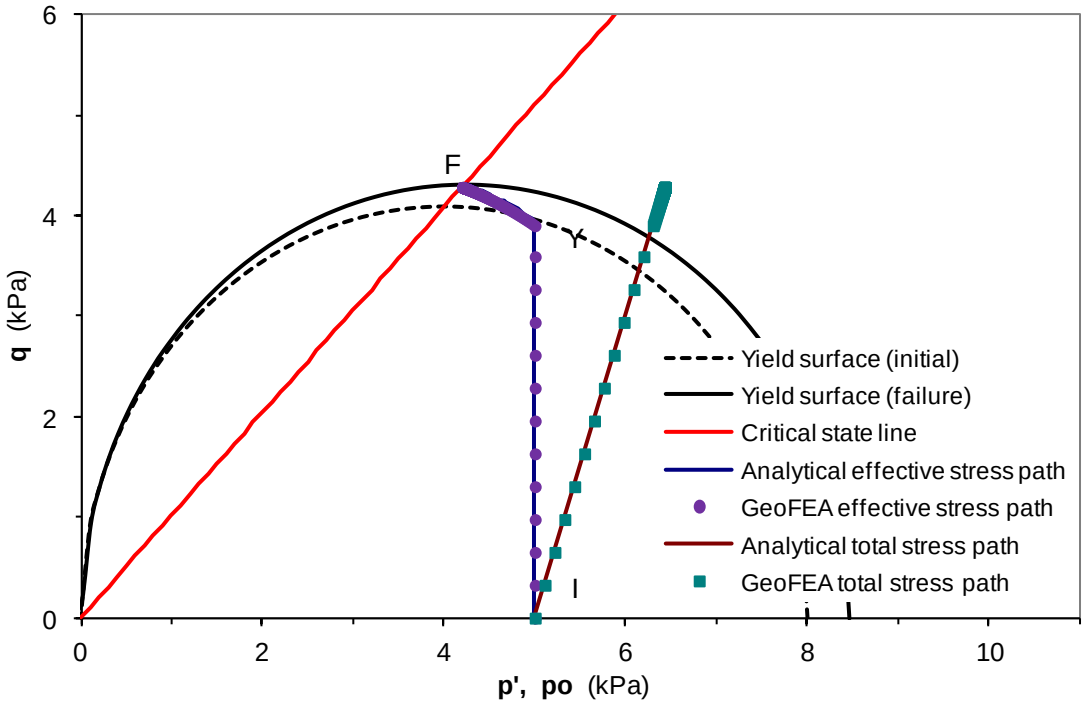


Figure 6-6 Total and effective stress paths in stress space for undrained test (OCR = 1.6)

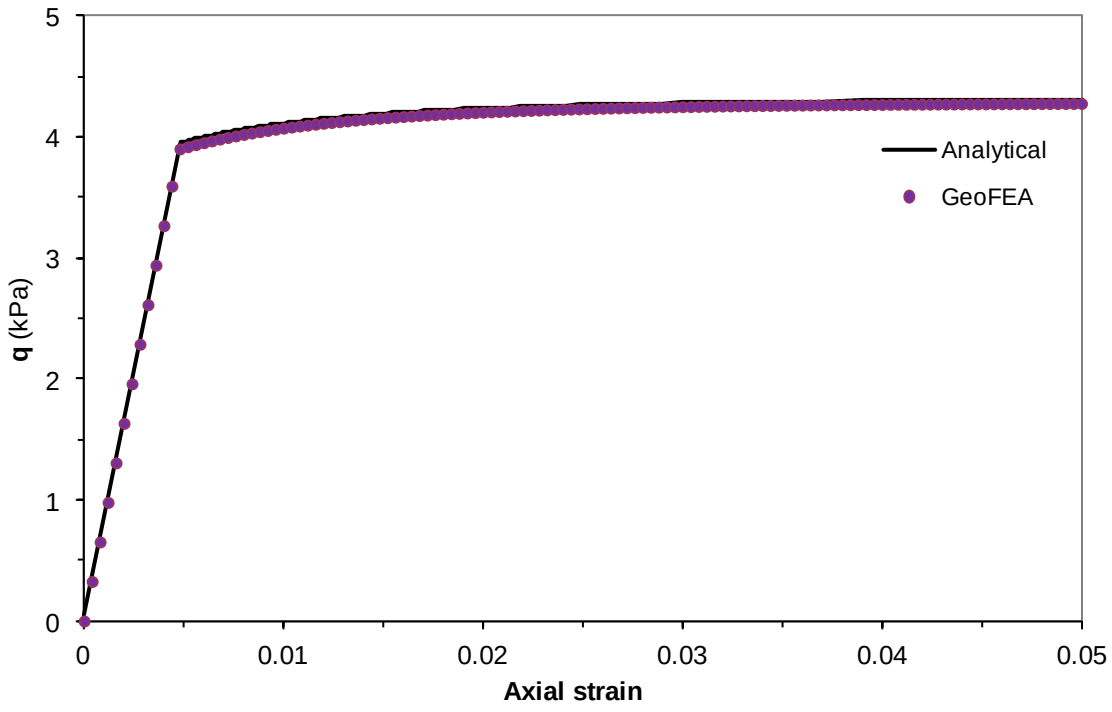


Figure 6-7 Relation between deviator stress and axial strain for undrained test (OCR = 1.6)

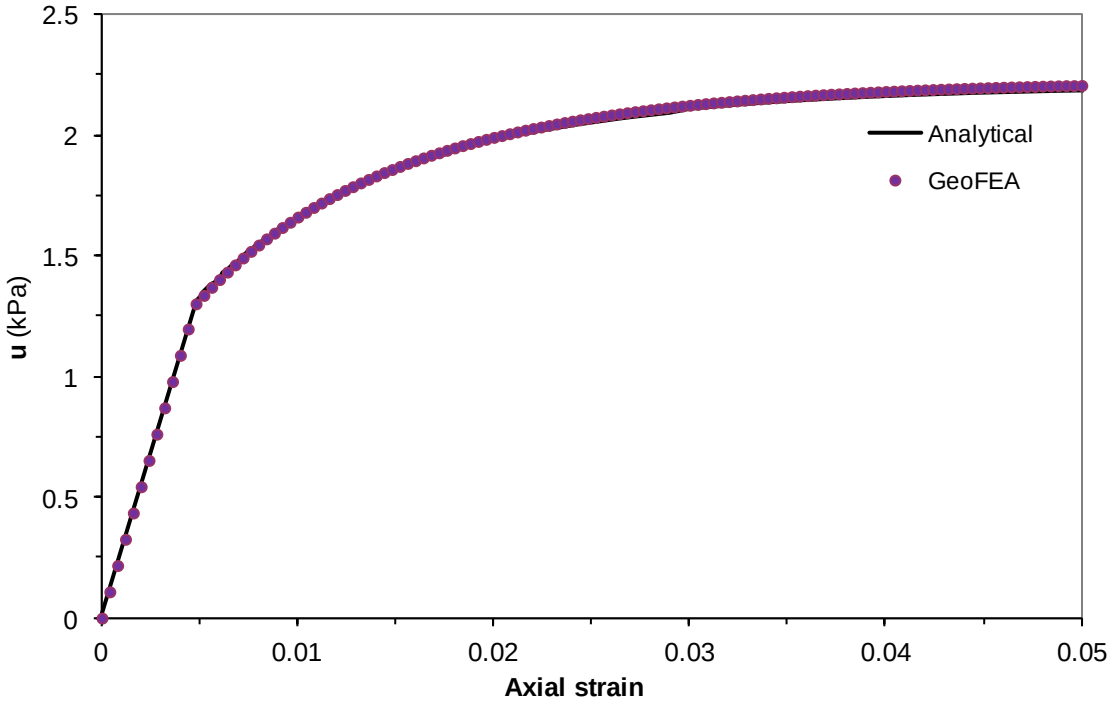


Figure 6-8 Relation between pore pressure and axial strain for undrained test (OCR = 1.6)

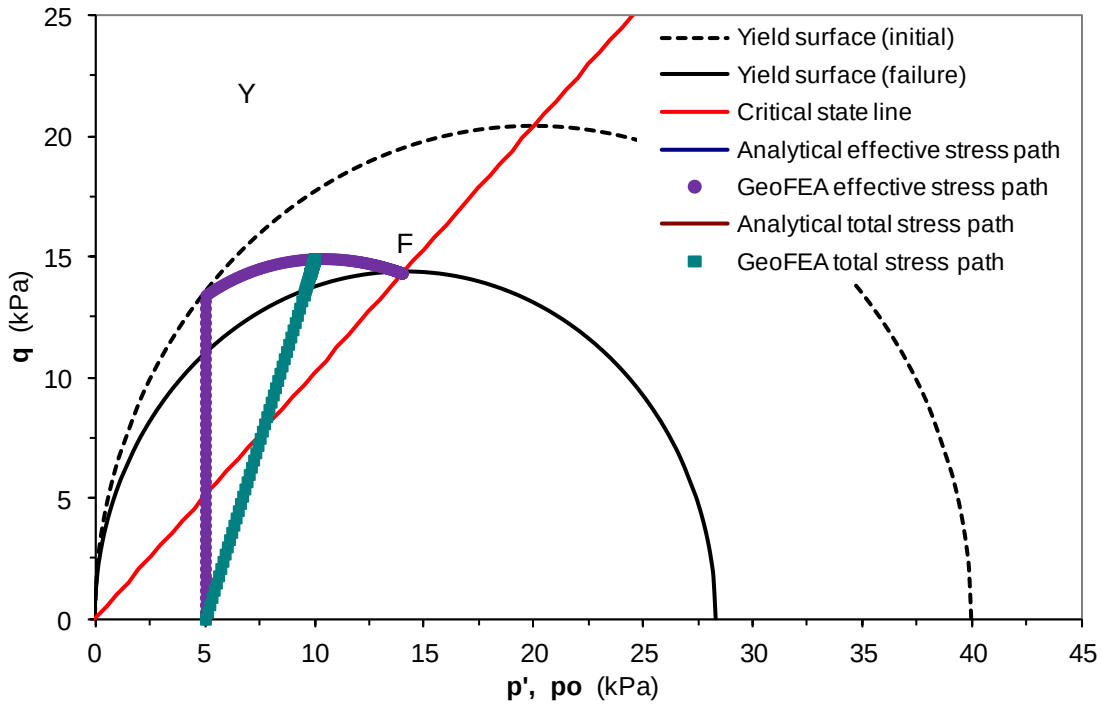


Figure 6-9 Total and effective stress paths in stress space for undrained test (OCR = 8.0)

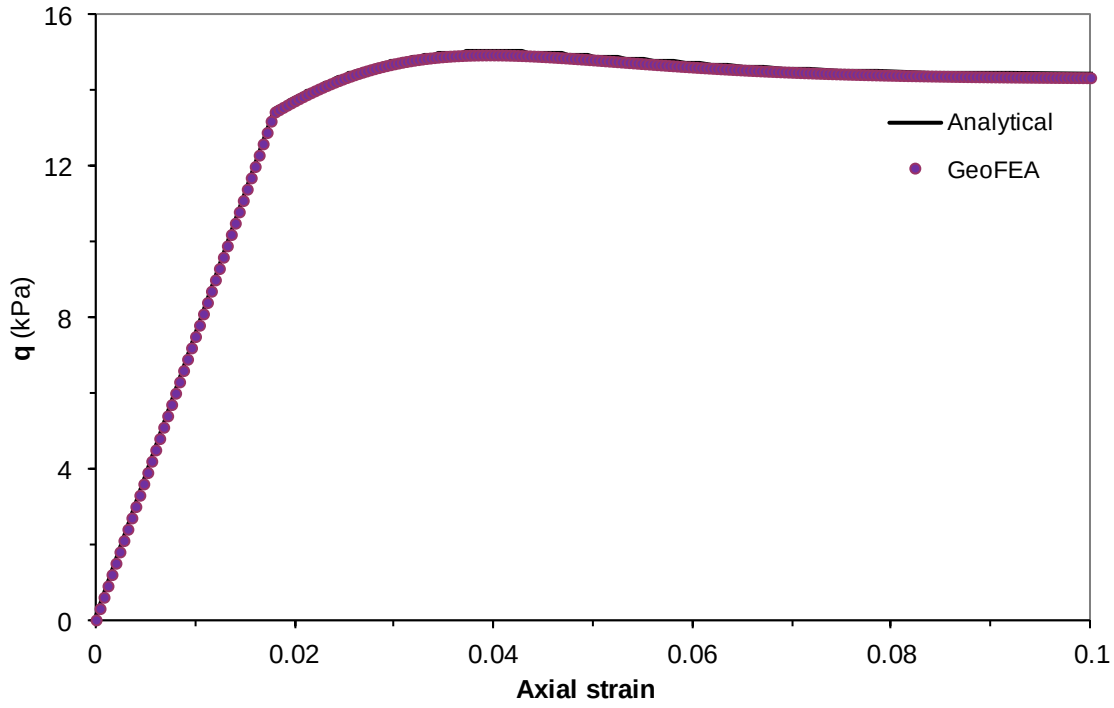


Figure 6-10 Relation between deviator stress and axial strain for undrained test (OCR = 8.0)

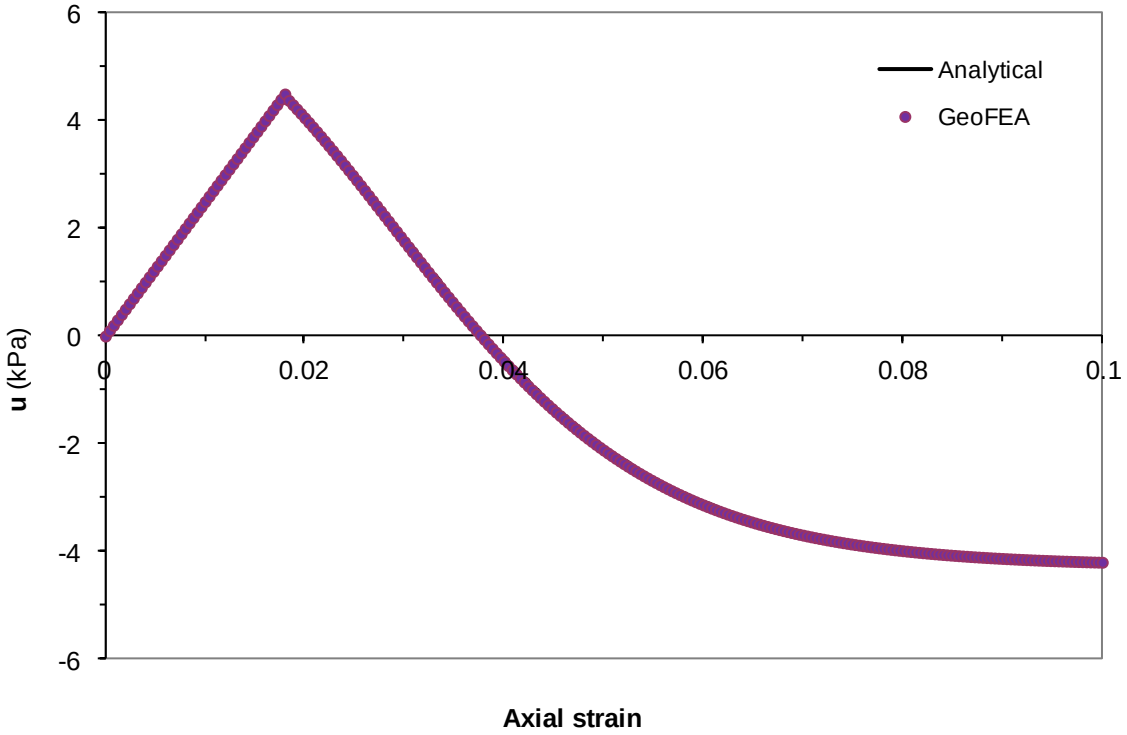


Figure 6-11 Relation between pore pressure and axial strain for undrained test (OCR = 8.0)

***Reference***

[1] R.I. Borja and S.R. Lee, (1990), Cam-Clay plasticity, part I: implicit integration of elasto-plastic constitutive relations, Computer Methods in Applied Mechanics and Engineering, 78, 49-72.
[2] D.M Wood, (1990), Soil Behaviour and Critical State Soil Mechanics. Cambridge, England: Cambridge University Press.

Redefining simplicity for geotechnical engineers

geofea®

GEOSOFT

Website: www.geosoft.sg